coatings

MDPI

Review

Electrodeposition of Calcium Phosphate Coatings on Metallic Substrates for Bone Implant Applications: A Review

Richard Drevet [1,*] and Hicham Benhayoune [2]

[1] Department of Physical Electronics, Masaryk University, Kotlářská 2, CZ-61137 Brno, Czech Republic
[2] Institut de Thermique, Mécanique et Matériaux (ITheMM), EA 7548, Université de Reims Champagne-Ardenne (URCA), Bât.6, Moulin de la Housse, BP 1039, CEDEX 2, 51687 Reims, France; hicham.benhayoune@univ-reims.fr
* Correspondence: richarddrevet@yahoo.fr

Abstract: This review summaries more than three decades of scientific knowledge on electrodeposition of calcium phosphate coatings. This low-temperature process aims to make the surface of metallic bone implants bioactive within a physiological environment. The first part of the review describes the reaction mechanisms that lead to the synthesis of a bioactive coating. Electrodeposition occurs in three consecutive steps that involve electrochemical reactions, pH modification, and precipitation of the calcium phosphate coating. However, the process also produces undesired dihydrogen bubbles during the deposition because of the reduction of water, the solvent of the electrolyte solution. To prevent the production of large amounts of dihydrogen bubbles, the current density value is limited during deposition. To circumvent this issue, the use of pulsed current has been proposed in recent years to replace the traditional direct current. Thanks to breaking times, dihydrogen bubbles can regularly escape from the surface of the implant, and the deposition of the calcium phosphate coating is less disturbed by the accumulation of bubbles. In addition, the pulsed current has a positive impact on the chemical composition, morphology, roughness, and mechanical properties of the electrodeposited calcium phosphate coating. Finally, the review describes one of the most interesting properties of electrodeposition, i.e., the possibility of adding ionic substituents to the calcium phosphate crystal lattice to improve the biological performance of the bone implant. Several cations and anions are reviewed from the scientific literature with a description of their biological impact on the physiological environment.

Keywords: electrodeposition; pulsed current; biomaterials; coating; calcium phosphate; hydroxyapatite; titanium; bone implant; ionic substitution

check for updates

Citation: Drevet, R.; Benhayoune, H. Electrodeposition of Calcium Phosphate Coatings on Metallic Substrates for Bone Implant Applications: A Review. *Coatings* **2022**, *12*, 539. https://doi.org/10.3390/coatings12040539

Academic Editor: Fabio Palumbo

Received: 24 March 2022
Accepted: 15 April 2022
Published: 17 April 2022

1. Introduction

The worldwide clinical demand for bone tissue repair increases every year, particularly due to the aging population [1–4]. The main metallic bone implants used in orthopedic or dental surgeries are titanium alloys [5–10], stainless steel [11–15], and CoCr alloys [16–22]. These alloys are used because they have suitable mechanical properties for bone tissue replacement and their biocompatibility with the body environment is good. According to the International Union of Pure and Applied Chemistry (IUPAC), biocompatibility is the ability of a material to be in contact with a biological system without producing an adverse effect [23–25]. Although these alloys are biocompatible with the body environment, their biological interaction with the bone tissues is very low. Without any improvement in the bioactivity of the implant surface, the bone anchor fails, and revision surgery is required. This is the reason why metal bone implants are commonly coated with calcium phosphate, a ceramic material with a chemical composition similar to that of bone mineral [26–32]. The bioactivity of the calcium phosphate surface layer stimulates the formation of a direct, adherent, and strong bond with bone tissue [33,34]. The calcium phosphate

coating initiates a rapid biological response and improves the adhesion of the implant to the bone by providing a scaffold for bone growth [35–37]. There are several methods to produce calcium phosphate coatings on implant surfaces, such as plasma spraying [38–45], magnetron sputtering [46–51], pulsed laser deposition [52–54], electrophoretic deposition [55–66], or electrodeposition [67–92]. Plasma spraying is the main coating process used in the bone-implant industry due to its ability to produce large quantities of coatings with good reproducibility. However, there are some drawbacks to plasma spraying because this process involves very high temperatures that induce uncontrolled phase changes and thermomechanical mismatches [40]. Electrodeposition is an alternative method for the synthesis of calcium phosphate coatings at low temperatures, first introduced by Shirkhanzadeh in 1991 [93–95]. For more than three decades, several research laboratories and companies around the world have regularly proposed new developments to improve the efficiency of this electrochemical process (Figure 1).

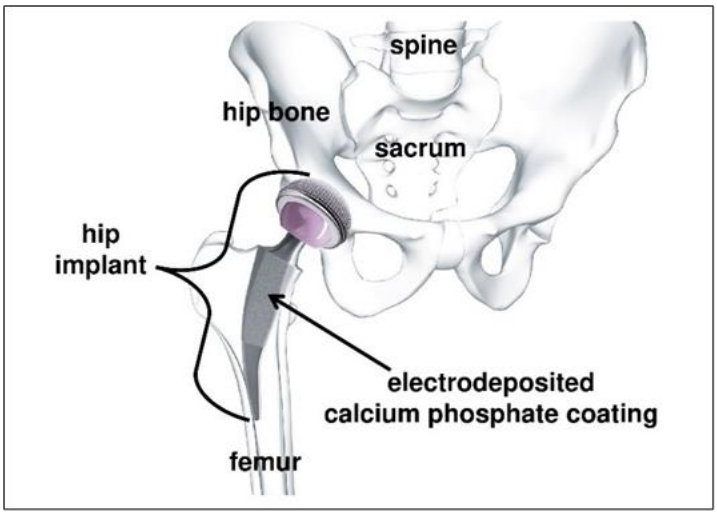

Figure 1. Industrial calcium phosphate coating electrodeposited on titanium hip implant. Reprinted and adapted with permission from Aesculap—BBraun Gmbh.

Electrodeposition uses electrical energy from a generator to trigger a series of chemical reactions in an aqueous solution, leading to the synthesis of a calcium phosphate coating on a conductive surface [85]. The direct current was typically used first for more than twenty years but pulsed current electrodeposition has grown in recent years. The main reason is that the pulsed current mode includes some break times during deposition, providing several benefits detailed in this review of the literature. The first section in-depth describes the reaction mechanisms involved during the electrodeposition process. The direct current and pulsed current modes are presented and compared in the following sections. The last part presents more specific developments of electrodeposition with some ionic additives to enhance the biological properties of the synthesized calcium phosphate coatings.

2. Electrodeposition of Calcium Phosphate Coatings

Electrodeposition is an electrochemical process that uses two electrodes immersed in an aqueous solution containing calcium and phosphate ions. Most experimental protocols use calcium nitrate tetrahydrate ($(CaNO_3)_2{\cdot}4H_2O$) and ammonium dihydrogen phosphate ($NH_4(H_2PO_4)$) to produce the electrolyte solution. The two electrodes are connected to an electrical generator (Figure 2).

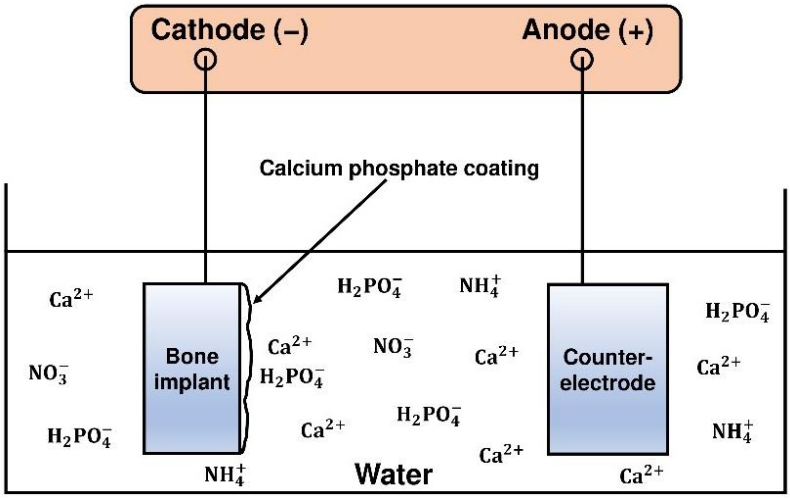

Figure 2. Sketch of the experimental setup used for electrodeposition.

In an electrolytic cell, the anode is the positive electrode, and the cathode is the negative electrode. When a current density is applied, the electrolysis of water (the solvent) triggers redox reactions on the surfaces of both electrodes. At the cathode where the metal bone implant is connected, the electrochemical reactions imply a pH variation that induces the surface precipitation of a calcium phosphate layer.

2.1. Electrochemical Reactions

Several redox reactions may occur at the two electrode-electrolyte interfaces. Oxidation reactions take place at the anode, and reduction reactions take place at the cathode. The main redox reactions of the process involve water, the solution solvent whose anodic oxidation is:

$$2H_2O \rightarrow O_2 \uparrow + 4H^+ + 4e^- \quad (1)$$

The cathodic reduction of water occurs simultaneously:

$$2H_2O + 2e^- \rightarrow H_2 \uparrow + 2OH^- \quad (2)$$

In an acidic medium, proton reduction can also take place at the cathode:

$$2H^+ + 2e^- \rightarrow H_2 \uparrow \quad (3)$$

These reduction reactions locally increase the pH value of the solution at the cathode-electrolyte interface, causing acid-base reactions. However, several authors also describe other electrochemical reactions that affect the local pH value in the vicinity of the cathode [69,96–98]:

$$O_2 + 2H_2O + 4e^- \rightarrow 4OH^- \quad (4)$$

$$O_2 + 2H_2O + 2e^- \rightarrow 2OH^- + H_2O_2 \quad (5)$$

$$NO_3^- + 2H^+ + 2e^- \rightarrow NO_2^- + H_2O \quad (6)$$

$$NO_3^- + 10H^+ + 8e^- \rightarrow NH_4^+ + 3H_2O \quad (7)$$

$$NO_3^- + H_2O + 2e^- \rightarrow NO_2^- + 2OH^- \quad (8)$$

$$NO_3^- + 7H_2O + 8e^- \rightarrow NH_4^+ + 10OH^- \quad (9)$$

$$NO_3^- + 6H_2O + 8e^- \rightarrow NH_3 + 9OH^- \quad (10)$$

$$H_2PO_4^- + H_2O + 2e^- \rightarrow H_2PO_3^- + 2OH^- \quad (11)$$

However, the amounts of oxygen, nitrate, and dihydrogen phosphate ions are very low compared to the amount of water, the solvent of the electrolyte solution. The reduction of

water or the reduction of protons are the main cathodic reactions during the electrochemical process. The corresponding pH variations in the vicinity of the cathode promote the dissociation of the dihydrogen phosphate ions according to an acid-base process.

2.2. Acid-Base Reactions

As prepared, the pH of the electrolyte solution is typically acid (4 < pH < 5). At the cathode-electrolyte interface, the variation of pH due to the reduction of water induces the dissociation of dihydrogen phosphate ions in the solution (Figure 3).

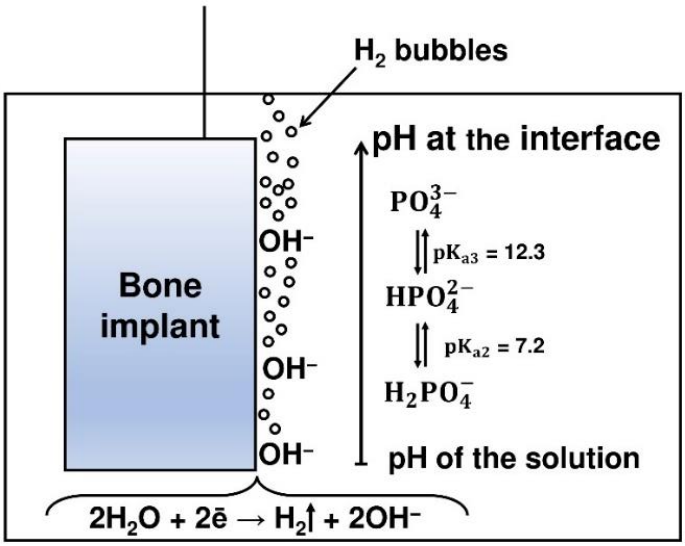

Figure 3. Sketch of the cathode-electrolyte interface during deposition.

The concentration of phosphate species as a function of the pH of the solution is shown in Figure 4.

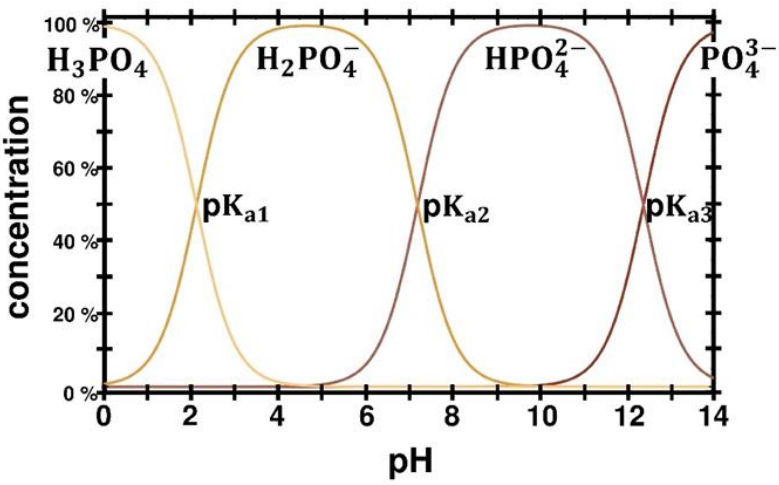

Figure 4. Concentration of phosphate species as a function of the pH value. Reprinted and adapted with permission from Ref. [99]. Copyright 2020 Clarolux.

With a pH value between 4 and 5, the electrolytic solution initially contains dihydrogen phosphate ions ($H_2PO_4^-$). When the local pH increases between 7.2 and 12.3 in the vicinity of the cathode, the hydrogen phosphate ions (HPO_4^{2-}) become the major phosphate ions produced according to reaction (12):

$$H_2PO_4^- \rightarrow HPO_4^{2-} + H^+ \quad (12)$$

For pH values greater than 12.3, the phosphate ions (PO_4^{3-}) predominate according to reaction (13):

$$HPO_4^{2-} \rightarrow PO_4^{3-} + H^+ \quad (13)$$

2.3. Calcium Phosphate Coating Precipitation

Reactions (12) and (13) induce a local ionic supersaturation that causes the precipitation of a calcium phosphate coating characterized by low solubility and high thermodynamic stability. As a function of the pH value in the vicinity of the cathode, various phases can precipitate:

- dicalcium phosphate dihydrate (brushite):

$$Ca^{2+} + HPO_4^{2-} + 2\,H_2O \rightarrow CaHPO_4{\cdot}2\,H_2O \quad (14)$$

- octacalcium phosphate:

$$8\,Ca^{2+} + 2\,HPO_4^{2-} + 4\,PO_4^{3-} + 5\,H_2O \rightarrow Ca_8(HPO_4)_2(PO_4)_4{\cdot}5\,H_2O \quad (15)$$

- calcium-deficient apatite:

$$(10-x)Ca^{2+} + xHPO_4^{2-} + (6-x)PO_4^{3-} + (2-x)OH^- \rightarrow Ca_{10-x}(HPO_4)_x(PO_4)_{6-x}(OH)_{2-x} \quad (16)$$

with $0 < x < 2$

- hydroxyapatite:

$$10\,Ca^{2+} + 6\,PO_4^{3-} + 2OH^- \rightarrow Ca_{10}(PO_4)_6(OH)_2 \quad (17)$$

The composition of the calcium phosphate coating depends on the pH value at the cathode, which is related to the current density imposed by the generator. The main characteristic of these calcium phosphate phases is their stoichiometry, specifically described in biomaterials science by their calcium to phosphorus atomic ratio (Ca/P). The stoichiometry of the phase is related to its solubility in a physiological environment, corresponding to the surface bioactivity conferred to the bone-implant (Table 1).

Table 1. Calcium phosphate coatings produced by electrodeposition.

Calcium Phosphate	Abbreviation	Chemical Formula	$(Ca/P)_{at.}$	Solubility $[-\log(K_s)]$	References
dicalcium phosphate dihydrate (brushite)	DCPD	$CaHPO_4{\cdot}2\,H_2O$	1.00	6.6	[100–102]
octacalcium phosphate	OCP	$Ca_8(HPO_4)_2(PO_4)_4{\cdot}5\,H_2O$	1.33	96.6	[103–105]
calcium-deficient apatite	Ca-def apatite	$Ca_{10-x}(HPO_4)_x(PO_4)_{6-x}(OH)_{2-x}$	1.34–1.66	85.1	[106–108]
β-tricalcium phosphate *	β-TCP	$\beta\text{-}Ca_3(PO_4)_2$	1.50	28.9	[109–111]
hydroxyapatite	HAP	$Ca_{10}(PO_4)_6(OH)_2$	1.67	116.8	[72,73,85]

* only after thermal annealing at T > 800 °C.

Experimentally, the phases of calcium phosphate are mostly identified by X-ray diffraction (Figure 5) and infrared spectroscopy (Figure 6).

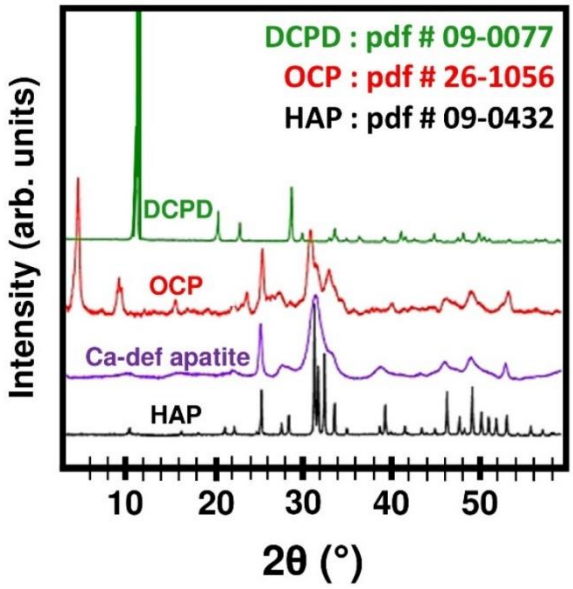

Figure 5. XRD patterns of electrodeposited calcium phosphate coatings. Reprinted and adapted with permission from Ref. [112]. Copyright 2013 Christophe Drouet.

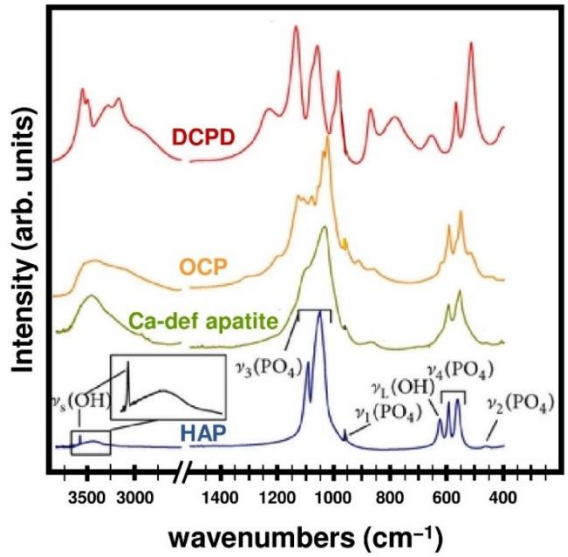

Figure 6. FT-IR spectra of electrodeposited calcium phosphate coatings. Reprinted and adapted with permission from Ref. [112].

Thermal annealing of calcium-deficient apatite ($Ca_{10-x}(HPO_4)_x(PO_4)_{6-x}(OH)_{2-x}$) at 800 °C produces a mixture of crystalline phases whose proportions depend on its stoichiometry, hence its Ca/P atomic ratio. The obtained crystallized material is a biphasic compound.

If the value of x is between 0 and 1, the calcium-deficient apatite phase has a Ca/P atomic ratio between 1.5 and 1.67. Crystallization of calcium-deficient apatite produces a mixture of HAP and β-tricalcium phosphate (β-TCP) according to reaction (18).

$$\underset{\text{Ca-def apatite}}{Ca_{10-x}(HPO_4)_x(PO_4)_{6-x}(OH)_{2-x}} \xrightarrow{800\ ^\circ C} \underset{(1-x)\ HAP + (3x)\ \beta\text{-TCP} + (x)\ H_2O}{(1-x)Ca_{10}(PO_4)_6(OH)_2 + (3x)Ca_3(PO_4)_2 + (x)\ H_2O} \quad (18)$$

If the value of x is exactly 1, the calcium to phosphorus atomic ratio is 1.5 and the calcium-deficient apatite phase is specifically named tricalcium phosphate (TCP). Thermal annealing at 800 °C crystallizes it into the β phase according to reaction (19) [113].

$$\underset{\text{TCP}}{Ca_9(HPO_4)(PO_4)_5(OH)} \xrightarrow{800\ ^\circ C} \underset{\beta\text{-TCP}}{3\ Ca_3(PO_4)_2} \quad (19)$$

The XRD pattern and the FT-IR spectrum of β-TCP are shown in Figures 7 and 8, respectively.

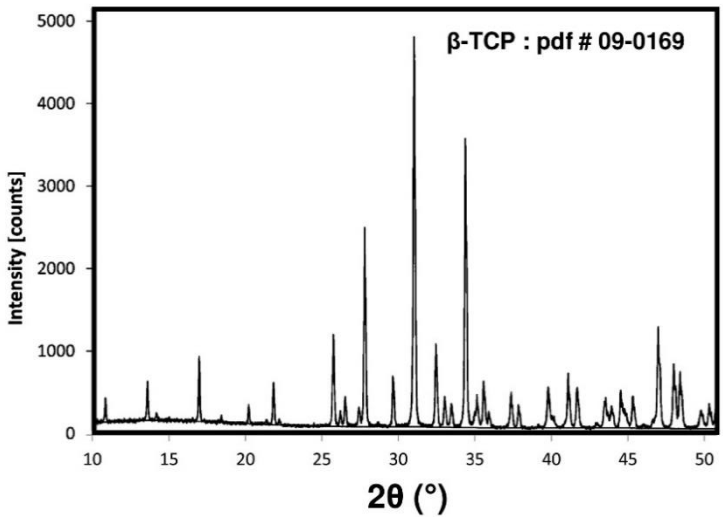

Figure 7. XRD pattern of β-TCP. Reprinted and adapted with permission from Ref. [114]. Copyright 2020 Elsevier.

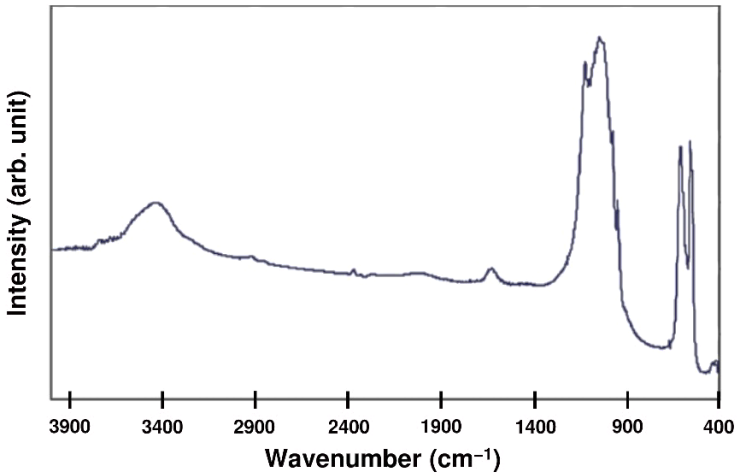

Figure 8. FT-IR spectrum of β-TCP. Reprinted and adapted with permission from Ref. [115]. Copyright 2017 Elsevier Masson SAS. All rights reserved.

3. Drawbacks of Direct Current Electrodeposition

Although electrodeposition is an efficient process to produce calcium phosphate coatings, there are several disadvantages and limitations to using it in a direct current mode.

3.1. Ionic Mobility

As described in Section 2.3, electrodeposited calcium phosphate coatings are obtained by precipitation of cations (Ca^{2+}) with anions (phosphates). Most of the protocols in the literature describe electrolytic solutions prepared with calcium salt and phosphate salt

whose molar concentrations have a ratio of 1.67. Typically, the concentration of calcium salt is 0.042 mol L^{-1} and the concentration of phosphate salt is 0.025 mol L^{-1}. This molar ratio is generally chosen with the perspective to produce hydroxyapatite ($Ca_{10}(PO_4)_6(OH)_2$), the gold standard among calcium phosphates, whose calcium to phosphorus atomic ratio is 1.67. However, despite this molar ratio in solution, very few articles show electrodeposited calcium phosphate coatings with the stoichiometry of hydroxyapatite. This could be the result of the mobility of the ions in the solution that modifies the local concentrations of calcium and phosphate ions in the vicinity of the electrodes. During the electrochemical process, the ions move under the influence of the electric field between the two electrodes. The cations move toward the cathode, and the anions move toward the anode [116,117]. The longer the deposition, the more local concentrations in the solution are modified and impact the stoichiometry of the electrodeposited coating. This implies a limitation of the process duration when electrodeposition is used in a direct current mode. This is one of the reasons why regular break times are necessary during deposition, to restore the initial electrolyte concentrations everywhere in the solution.

3.2. Accumulation of Dihydrogen Bubbles

The main electrochemical reaction involved in the process is the reduction of water according to reaction (2). This reaction produces dihydrogen bubbles on the surface of the cathode, where the deposition of the coating is expected. Most of the dihydrogen bubbles escape quickly from the cathode, but some of them remain adsorbed on the surface. These bubbles prevent uniform deposition and promote the formation of many porosities that reduce the mechanical properties of the calcium phosphate coating. The cohesion of the layer and its adhesion to the substrate are particularly impacted. The SEM image of Figure 9 shows an example of the porosities caused by adsorbed dihydrogen bubbles on a calcium phosphate coating electrodeposited in direct current mode.

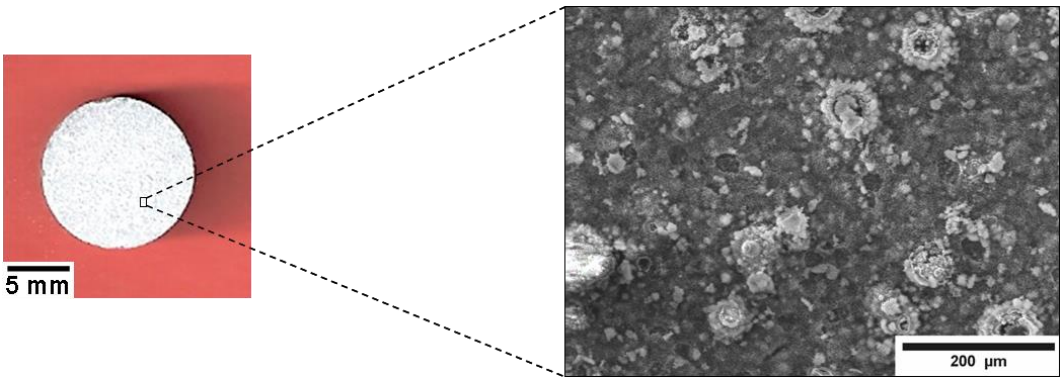

Figure 9. Photograph and SEM image of a calcium phosphate coating electrodeposited with direct current at 15 mA cm^{-2}. Reprinted with permission from Ref. [72]. Copyright 2010 Wiley.

The higher the current density, the more dihydrogen bubbles are produced [118]. Therefore, the maximum current density value is limited by the number of bubbles produced by the process. This implies a limitation of the pH values reachable in the vicinity of the cathode, i.e., a limitation of the chemical compositions the process can produce. Since dihydrogen bubbles impose some limitations on the stoichiometry of the synthesized calcium phosphate coatings, the surface bioactivity of the implant is affected. This is one of the reasons why regular break times are necessary during deposition to reduce the accumulation of disturbing dihydrogen bubbles on the surface of the cathode.

4. Advantages of Pulsed Current Electrodeposition

The use of pulsed current is an efficient solution to solve the problems described above. The idea is to provide some regular break times (t_{off}) during deposition (t_{on}) to restore the initial experimental conditions (Figure 10).

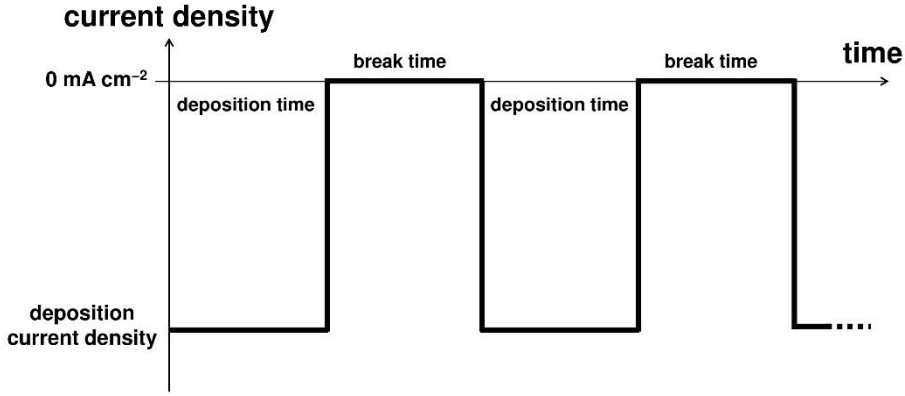

Figure 10. Sketch of the pulsed current.

Different experimental protocols for pulsed currents are described in the literature, with short or long break times. Most protocols describe deposition times and break times of the same duration, but longer break times are also possible. Various durations can be used, ranging from a few microseconds to tens of seconds [72–75,119–121]. However, in all these works, the authors note several advantages of using pulsed currents, describing the improved properties of the electrodeposited calcium phosphate coatings. The authors describe more uniform calcium phosphate coatings with less porosity (Figure 11).

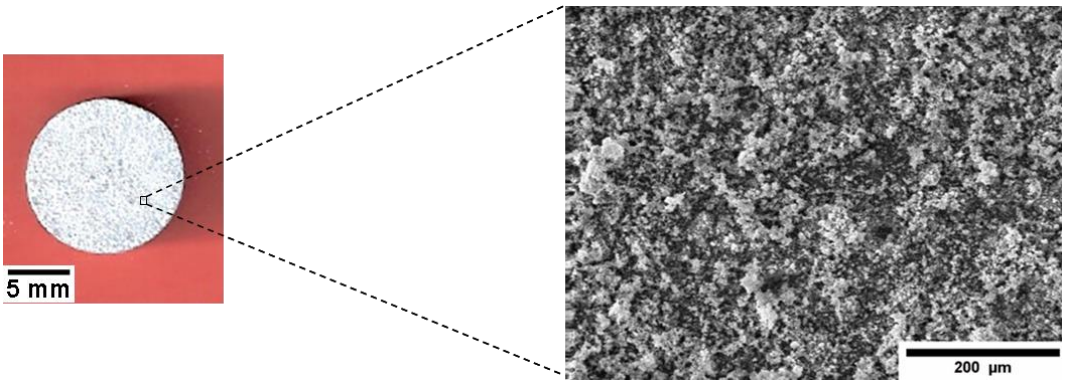

Figure 11. Photograph and SEM image of a calcium phosphate coating electrodeposited with pulsed current at 15 mA cm^{-2}. Reprinted with permission from Ref. [72]. Copyright 2010 Wiley.

4.1. Higher Current Densities

As previously described, the current density values are limited because of their impact on the local ionic concentrations in the solution and on the number of dihydrogen bubbles produced. Both phenomena are undesirable and must be reduced to ensure appropriate electrodeposition of calcium phosphate coatings.

When electrodeposition is carried out in direct current mode, current densities are limited to a maximum of 10 mA cm^{-2} [122]. Beyond this value, the generated dihydrogen bubbles damage the electrodeposited coating [118]. This maximum current density can be used to produce a calcium-deficient apatite according to reaction (16). Typically, this phase has a calcium to phosphorus atomic ratio between 1.5 and 1.6. After post-deposition thermal annealing at a temperature higher than 800 °C, calcium-deficient apatite crystallizes into a biphasic compound made of hydroxyapatite and β-tricalcium phosphate according to reaction (18) [109]. The proportion of each crystallized phase depends on the stoichiometry of the calcium-deficient apatite, which is described by its calcium to phosphorus atomic ratio.

When electrodeposition is used in a pulsed current mode, the regular break times during the process are efficient for homogenizing the electrolyte solution and letting the dihydrogen bubbles escape from the cathode surface. Therefore, the impact of the two unfavorable phenomena is reduced. The range of usable current densities increases, giving access to an

extended range of chemical compositions. Current densities of up to 15 mA cm^{-2} can be used to reach higher pH values and reduce the calcium deficiency of the apatite coating. Another solution to further increase the pH value in the vicinity of the cathode consists of adding hydrogen peroxide (H_2O_2) to the electrolyte solution. Hydrogen peroxide is a strong oxidative reagent whose reduction at the cathode produces hydroxide ions according to the reaction (20):

$$H_2O_2 + 2e^- \rightarrow 2\,OH^- \quad (20)$$

However, the amount of hydrogen peroxide in the electrolytic solution is limited to avoid the overproduction of hydroxide ions that prevent an appropriate deposition of the coating [123]. When combining an optimized pulsed current with a 9 vol.% H_2O_2 concentration, a stoichiometric hydroxyapatite coating with a calcium to phosphorus atomic ratio of 1.67 is produced according to reaction (17). The obtained coating is less porous and composed of thin needles agglomerates that form spheroids of 1 µm in diameter. This means that the process can be used to produce all the calcium phosphate phases shown in Table 1 or a mixture of these phases. The low current densities of about 1 mA cm^{-2} produce brushite [122]. Intermediate current densities with values ranging from 2 mA cm^{-2} to 15 mA cm^{-2} produce octacalcium phosphate and calcium-deficient apatite [111]. Therefore, the combination of a current density of 15 mA cm^{-2} and hydrogen peroxide produces stoichiometric hydroxyapatite [72,73,85]. The bioactivity of the calcium phosphate coating can be chosen from a more soluble and reactive compound (brushite) to a more stable material (hydroxyapatite). This flexibility in composition gives full control over the kinetics of interactions between the bone-implant and the body environment, i.e., full control over the bioactivity of the biomaterial.

4.2. Improved Morphology and Roughness

The electrodeposited calcium phosphate coatings are made of crystallites that grow during deposition. The direct current mode produces crystallites that have the morphology of needles of about 1 µm in size stacked one upon another (Figure 12). Sharp microneedles are harmful to bone cells, preventing attachment and spreading [124,125].

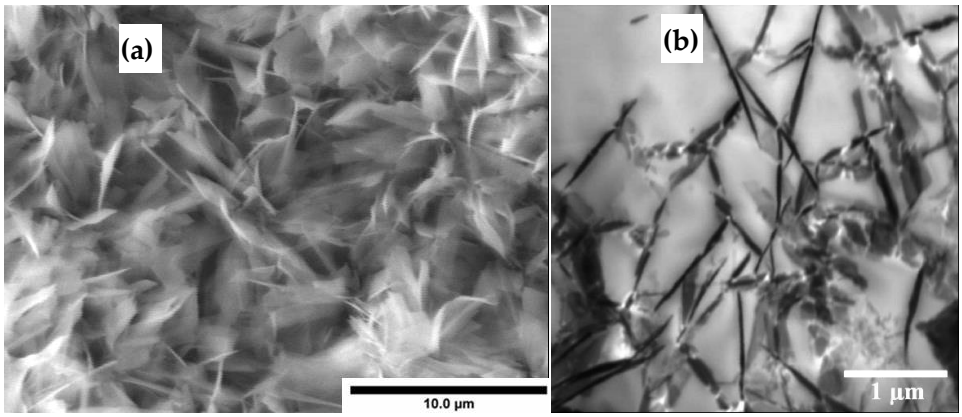

Figure 12. Calcium phosphate coating obtained by direct current electrodeposition. (**a**) SEM image and (**b**) TEM image. Reprinted with permission from Ref. [85]. Copyright 2012 Nova Science Publishers.

On the other hand, pulsed current electrodeposition produces smaller crystallites that agglomerate to form spheroids (Figure 13).

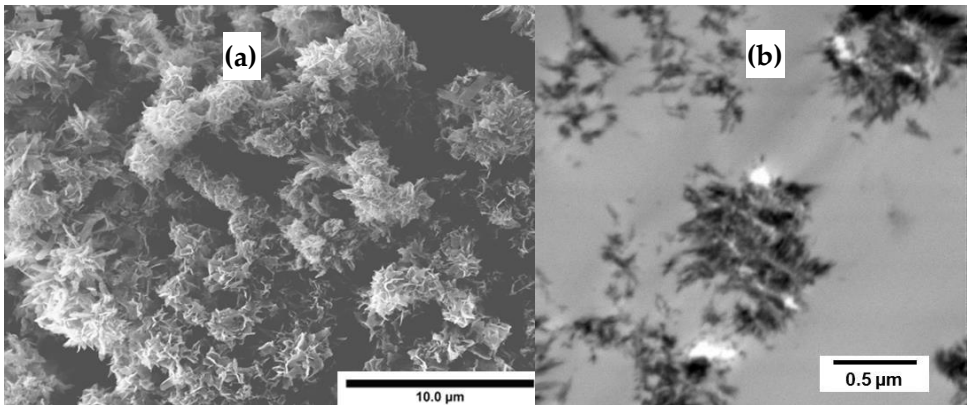

Figure 13. Calcium phosphate coating obtained by pulsed current electrodeposition. (**a**) SEM image and (**b**) TEM image. Reprinted with permission from Ref. [74]. Copyright 2011 Springer US.

This characteristic morphology is more beneficial to bone cells and induces a decrease in the roughness of the coating. Morphology and roughness are two key parameters of calcium phosphate coatings, which are known to affect cell adhesion, spreading, proliferation, and differentiation. However, osteoblastic cell adhesion is a complex phenomenon and not only a simple physical attachment of cells [126,127]. Surface roughness is necessary, but only in a specific range. Roughness values greater than 2 µm inhibit osteoblastic cell adhesion because the long distances between the peaks and valleys are unfavorable to the formation of osteoblastic pseudopodia [128,129]. Cairns et al. explain that regular smooth topography significantly increases osteocalcin expression and alkaline phosphatase activity, which promote bone cell growth [130]. Valleys are necessary to promote cell localization and stretch, and peaks of appropriate size are suitable to facilitate cell adhesion. Pulsed electrodeposition produces calcium phosphate coatings with roughness values of ca. 1 µm and below, which is in the range of the most appropriate values for the best cell behavior [131,132].

4.3. Enhanced Mechanical Properties

Because of the break times during electrodeposition in pulsed current mode, the dihydrogen bubbles produced by the reduction of water can easily escape from the cathode surface. The nucleation and growth of the calcium phosphate coatings are less disturbed by the bubbles, resulting in the densification of the electrodeposited coatings. Scratch test and nanoindentation measurements show that pulsed electrodeposition improves adhesion, apparent Young's modulus, and hardness of calcium phosphate coatings compared to those obtained in direct current mode [133].

Post-deposition thermal annealing can be used to densify the coating [134–136]. Temperatures up to 550 °C are generally used for air treatments to avoid oxidation of the metallic substrate. Under a controlled atmosphere (e.g., argon or vacuum), temperatures up to 1000 °C have been described [111]. The corresponding improvement in adhesion is generally studied by a standardized measurement of tensile adhesion according to the international standard ISO 13779-4 (Figure 14) [137].

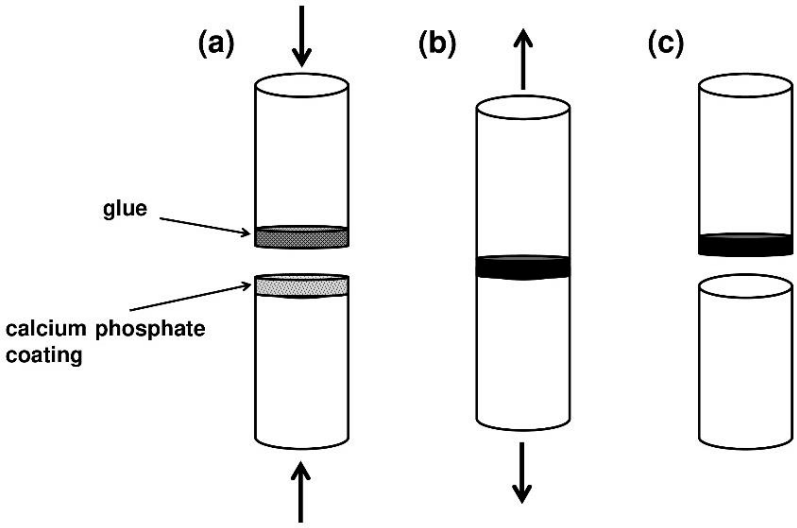

Figure 14. Sketch of the standardized measurement of tensile adhesion.

Briefly, a Ti6Al4V cylinder (25 mm in diameter and 25 mm in height) is coated with calcium phosphate and the coated surface is pasted against another Ti6Al4V cylinder coated with adhesive glue (Figure 14a). After polymerization of the glue, the system is exposed to an increasing load applied by a standard tensile machine (Figure 14b) until a total removal of the coating (Figure 14c). The test is repeated five times to obtain an average adhesion value. The resulting adhesion values must be greater than 15 MPa to be accepted by the bone-implant industry [138].

5. Ionic Substitution to Enhance the Properties of Electrodeposited Coatings

A powerful property of electrodeposition is the possibility of adding ionic substituents to the electrolyte solution used for the synthesis. During deposition, the ionic substituents are integrated into the calcium phosphate lattice to enhance the biological properties of the coating. Several ions are described in the scientific literature with different biological effects [139–147].

5.1. Divalent Cations

The most common substitutions of electrodeposited calcium phosphate coatings are obtained from divalent cations (M^{2+}) substituting calcium (Ca^{2+}) according to reaction (21):

$$(10-x)Ca^{2+}+xM^{2+}+yHPO_4^{2-}+(6-y)PO_4^{3-}+2OH^- \rightarrow Ca_{10-x}M_x(HPO_4)_y(PO_4)_{6-y}(OH)_2 \quad (21)$$

Among the divalent cations capable of enhancing the biological properties of electrodeposited calcium phosphate coatings, Co^{2+}, Cu^{2+}, Mg^{2+}, Mn^{2+}, Sr^{2+}, Zn^{2+} are particularly studied in the scientific literature.

5.1.1. Cobalt (Co^{2+})

The addition of cobalt to the calcium phosphate coating aims to promote angiogenesis in vivo, i.e., the neovascularization of newly formed bone tissues. These new blood vessels are involved in the supply of nutrients to bone cells and the transport of macromolecules during bone repair and regeneration [148]. For the efficient promotion of angiogenesis and to prevent any toxic effect of cobalt ions within the body, a 5 at.% substitution is commonly recommended [149].

5.1.2. Copper (Cu^{2+})

Copper is well known to provide antibacterial properties to various surfaces, particularly against *Escherichia coli* (*E. coli*) strains [150]. Copper reduces the permeability

of the cell membrane of bacteria, preventing their replication, and finally causing their death [151]. However, the amount of copper in the physiological environment must be limited to prevent any toxic effect on bone cells at high concentrations [152].

5.1.3. Magnesium (Mg^{2+})

Magnesium is known to promote bone densification. An appropriate amount of magnesium in the implant coating improves osteoblastic cell attachment and proliferation. Magnesium also increases the production of alkaline phosphatase, the main enzyme involved in the mineralization of the extracellular matrix of bone [153–156].

5.1.4. Manganese (Mn^{2+})

Manganese is mainly described for its ability to regulate osteoblast differentiation, control bone resorption, and promote cell adhesion [157]. Furthermore, manganese ions promote the production of osteocalcin, a protein produced by osteoblasts and involved in the bone formation process [158].

5.1.5. Strontium (Sr^{2+})

The use of strontium is well known in the form of strontium ranelate, a widely used drug for the treatment of bone defects such as postmenopausal osteoporosis. Strontium stimulates bone formation and inhibits bone resorption, which explains the increase in bone density in patients [159,160]. A 5 at.% substitution shows the best results in osteoblast cell activity and differentiation, and in osteoclast cell proliferation [161–163].

5.1.6. Zinc (Zn^{2+})

Zinc in calcium phosphate coatings is described for several biological actions. Zinc mainly provides antibacterial and anti-inflammatory properties, but the promotion of bone formation and regeneration is also described in the literature [164]. Bone cell adhesion and viability are generally improved due to the presence of a few percent of zinc in the calcium phosphate coatings [165,166].

5.2. Monovalent Cations

Several monovalent cations are also described for their interesting biological action.

5.2.1. Potassium (K^{+})

Potassium can activate several enzymes involved in the bone mineralization process [167–169]. Potassium also promotes cell adhesion and regulates biomechanical processes in bone minerals [170–172].

5.2.2. Silver (Ag^{+})

Silver is well-known to provide remarkable antibacterial properties to various surfaces. The bacterial inhibition is due to the ability of silver to penetrate the cytoplasm of bacteria. Silver can interact with thiol groups in proteins, inhibiting cellular respiration and causing the death of bacteria [173]. Another mechanism is attributed to the ability of silver to bind to microbial DNA to prevent bacterial replication [174,175].

5.2.3. Sodium (Na^{+})

Substitution with sodium ions enhances the biomineralization capacity of calcium phosphates in the physiological environment. Moreover, the positive contribution of sodium to bone cell adhesion and proliferation has been observed in vivo [176,177].

5.3. Anions

Anionic substitutions are described in the scientific literature in the case of hydroxyapatite. Anions can substitute phosphate groups to produce $Ca_{10}(PO_4)_{6-x}M_x(OH)_2$

compounds or hydroxyl groups to produce $Ca_{10}(PO_4)_6M_x(OH)_{2-x}$ [146]. The most common anions used to substitute electrodeposited calcium phosphate coatings are CO_3^{2-}, Cl^-, F^-, and SiO_4^{4-}.

5.3.1. Carbonate (CO_3^{2-})

Carbonate ions are naturally present in electrolyte solutions at room temperature because atmospheric carbon dioxide (CO_2) dissolves in water to produce carbonic acid (H_2CO_3) according to reaction (22).

$$CO_2 + H_2O \rightarrow H_2CO_3 \tag{22}$$

Carbonic acid is a weak dibasic acid characterized by two dissociation constants, $pKa_1 = 6.8$ and $pKa_2 = 9.9$. When the pH of the electrolyte solution increases, bicarbonate ions (HCO_3^-) and carbonate ions (CO_3^{2-}) are formed [85]:

$$H_2CO_3 \rightarrow HCO_3^- + H^+ \tag{23}$$

$$HCO_3^- \rightarrow CO_3^{2-} + H^+ \tag{24}$$

The chemical composition of carbonate calcium phosphates is very similar to that of bone apatite. Substitution with carbonate ions induces higher solubility and bioactivity of the calcium phosphate coating in the physiological environment [80,178,179].

5.3.2. Fluorine (F^-)

The use of fluorine is widespread in tooth care products to provide antibacterial properties. Substituting calcium phosphates with fluorine also stimulates the formation of the extracellular matrix and significantly improves bone cell proliferation and alkaline phosphatase activity [180,181].

5.3.3. Silicates (SiO_4^{4-})

Calcium phosphate substituted with silicates improves osteoblast attachment, proliferation, and differentiation. Silicates also favor the formation of extracellular matrix and increase alkaline phosphatase activity and osteocalcin expression [182,183].

5.4. Next Generation of Substituted Calcium Phosphate Coatings

Due to the variety of biological behaviors previously described, the multi-substitution of calcium phosphate coatings is an attractive solution to combine several biological properties of different ions [184–193]. For example, Bracci et al. describe multi-substitution with three divalent cations (Mg^{2+}, Sr^{2+}, and Mn^{2+}) to cumulate their positive impact on bone cell activity [194]. Another development proposed by Furko et al. is the electrodeposition of calcium phosphate coatings substituted with Ag^+ and Zn^{2+} to provide simultaneous antibacterial and anti-inflammatory properties to the surface of the bone-implant [195]. They also experiment with multi-elemental substitution of electrodeposited calcium phosphate coatings [196,197]. Other works describe electrodeposited calcium phosphate coatings that are simultaneously substituted by anions and cations. Olivier et al. use CO_3^{2-} and Sr^{2+} to produce coatings with a biomimetic chemical composition capable of improving bone cell proliferation [80]. Huang et al. substitute calcium phosphate coatings with F^- and Sr^{2+} to provide antibacterial properties and improve bone formation [198]. Bir et al. combine the antibacterial effects provided by F^- and Ag^+ to inhibit more bacterial growth on the surface of the bone-implant [199]. Many other combinations remain to be explored with different amounts of cations and anions added to the calcium phosphate crystal lattice. Ideally, the resulting coating will combine all the biological enhancements previously described (Table 2).

Table 2. Main ions used to substitute electrodeposited calcium phosphate coatings.

Ions	Salt	Electrolyte Concentration	Electrodeposition Mode	Biological Effect	Reference
divalent cations	-	-	-	-	-
Co^{2+}	$Co(NO_3)_2{\cdot}6H_2O$	0.525 to 4.20 mM	pulsed current	angiogenesis	[149]
Cu^{2+}	$Cu(NO_3)_2{\cdot}3H_2O$	0.167 mM	pulsed current	antibacterial activity	[152]
Mg^{2+}	$Mg(NO_3)_2{\cdot}6H_2O$	1.05 to 2.10 mM	pulsed current	bone formation	[156]
Mn^{2+}	$Mn(NO_3)_2{\cdot}4H_2O$	0.30 mM	direct current	bone formation	[158]
Sr^{2+}	$Sr(NO_3)_2$	1.02 to 4.20 mM	pulsed current	bone formation	[163]
Zn^{2+}	$Zn(NO_3)_2{\cdot}6H_2O$	5.0 to 10.0 mM	pulsed current	bone formation/antibacterial	[166]
monovalent cations	-	-	-	-	-
K^+	KCl	5.37 mM	direct current	bone formation	[172]
Ag^+	$AgNO_3$	10.0 mM	pulsed current	antibacterial activity	[175]
Na^+	$NaNO_3$	60.0 mM	cathodic polarization	bone formation	[177]
anions	-	-	-	-	-
CO_3^{2-}	no salt (see Section 5.3)	-	direct current	bioactivity	[179]
F^-	NaF	1.0 to 16.0 mM	direct current	antibacterial activity	[181]
SiO_4^{4-}	$Na_2SiO_3{\cdot}9H_2O$	2.5 to 7.5 mM	pulsed current	bioactivity	[183]

Another possible development is the substitution with new ions, already described in the literature to substitute calcium phosphate materials, but never in the case of electrodeposited coatings. For example, iron (Fe^{2+} or Fe^{3+}) is known to improve osteogenesis, simultaneously providing anticancer and antibacterial properties to calcium phosphates [200–202]. Chloride ions (Cl^-) are known to promote cell proliferation and osteoconductivity because of their ability to develop an acidic environment on the surface of bones. This acidity supports the action of osteoclasts in the bone resorption process [203–205]. Lithium (Li^+) improves bone regeneration by promoting alkaline phosphatase and osteogenic gene expression in osteoblasts [206,207]. Cerium (Ce^{3+} or Ce^{4+}) is used for effective antibacterial properties against *E. coli* and *S. aureus* [208,209]. Bismuth (Bi^{3+}), gallium (Ga^{3+}), and selenium (SeO_3^{2-}) show simultaneous positive impacts against bacteria and tumor cells [210–216]. Erbium (Er^{3+}), europium (Eu^{3+}), or terbium (Tb^{3+}) are added for their photoluminescence properties used in biological imaging systems [217–222]. The variety of all these ions and their biological impacts on calcium phosphate coatings used for bone implant applications will be part of the upcoming developments of the electrodeposition process.

6. Conclusions

In this review, the three steps to synthesize calcium phosphate coatings by electrodeposition were described: electrochemical reactions, acid-base reactions, and precipitation reactions. The process has limitations in the direct current mode because of the production of undesired dihydrogen bubbles due to the reduction of water, the solvent of the electrolyte solution. To solve this problem, pulsed current electrodeposition is a relevant solution that produces uniform calcium phosphate coatings with improved morphology, roughness, and mechanical properties. Moreover, the addition of hydrogen peroxide to the electrolytic solution provides more control over the chemical composition of the coating. Finally, the ionic substitution of electrodeposited calcium phosphate coatings was reviewed, and some new perspectives on the process were described. Multi-substitution or substitution with new ions will be the next development to improve the process.

Author Contributions: Conceptualization, R.D. and H.B.; methodology, R.D. and H.B.; validation, R.D. and H.B.; investigation, R.D. and H.B.; resources, R.D. and H.B.; writing—original draft preparation, R.D. and H.B.; writing—review and editing, R.D. and H.B. All authors have read and agreed to the published version of the manuscript.

Funding: This research received no external funding.

Institutional Review Board Statement: Not applicable.

Informed Consent Statement: Not applicable.

Data Availability Statement: Not applicable.

Conflicts of Interest: The authors declare no conflict of interest.

References

1. Demontiero, O.; Vidal, C.; Duque, G. Aging and bone loss: New insights for the clinician. *Ther. Adv. Musculoskel. Dis.* **2012**, *4*, 61–76. [CrossRef] [PubMed]
2. Gheno, R.; Cepparo, J.M.; Rosca, C.E.; Cotton, A. Musculoskeletal Disorders in the Elderly. *J. Clin. Imaging Sci.* **2012**, *2*, 39. [CrossRef] [PubMed]
3. U.S. Department of Health and Human Services. *Bone Health and Osteoporosis: A Report of the Surgeon General*; US Department of Health and Human Services, Office of the Surgeon General: Rockville, MD, USA, 2004.
4. Li, G.; Thabane, L.; Papaioannou, A.; Ioannidis, G.; Levine, M.A.H.; Adachi, J.D. An overview of osteoporosis and frailty in the elderly. *BMC Musculoskelet. Disord.* **2017**, *18*, 46. [CrossRef] [PubMed]
5. Farrakhov, R.; Melnichuk, O.; Parfenov, E.; Mukaeva, V.; Raab, A.; Sheremetyev, V.; Zhukova, Y.; Prokoshkin, S. Comparison of Biocompatible Coatings Produced by Plasma Electrolytic Oxidation on cp-Ti and Ti-Zr-Nb Superelastic Alloy. *Coatings* **2021**, *11*, 401. [CrossRef]
6. Ijaz, M.F.; Laillé, D.; Héraud, L.; Gordin, D.M.; Castany, P.; Gloriant, T. Design of a novel superelastic Ti-23Hf-3Mo-4Sn biomedical alloy combining low modulus, high strength and large recovery strain. *Mater. Lett.* **2016**, *177*, 39–41. [CrossRef]
7. Sheremetyev, V.; Dubinskiy, D.; Kudryashova, A.; Prokoshkin, S.; Brailovski, V. In situ XRD study of stress- and cooling-induced martensitic transformations in ultrafine- and nano-grained superelastic Ti-18Zr-14Nb alloy. *J. Alloys Compd.* **2022**, *902*, 163704. [CrossRef]
8. He, G.; Hagiwara, M. Ti alloy design strategy for biomedical applications. *Mater. Sci. Eng. C* **2006**, *26*, 14–19. [CrossRef]
9. Geetha, M.; Singh, A.K.; Asokamani, R.; Gogia, A.K. Ti based biomaterials, the ultimate choice for orthopaedic implants—A review. *Prog. Mater. Sci.* **2009**, *54*, 397–425. [CrossRef]
10. Chen, Q.; Thouas, G.A. Metallic implant biomaterials. *Mater. Sci. Eng. R* **2015**, *87*, 1–57. [CrossRef]
11. Drevet, R.; Zhukova, Y.; Malikova, P.; Dubinskiy, S.; Korotitskiy, A.; Pustov, Y.; Prokoshkin, S. Martensitic Transformations and Mechanical and Corrosion Properties of Fe-Mn-Si Alloys for Biodegradable Medical Implants. *Metall. Mater. Trans. A* **2018**, *49*, 1006–1013. [CrossRef]
12. Drevet, R.; Zhukova, Y.; Kadirov, P.; Dubinskiy, S.; Kazakbiev, A.; Pustov, Y.; Prokoshkin, S. Tunable corrosion behavior of calcium phosphate coated Fe-Mn-Si alloys for bone implant applications. *Metall. Mater. Trans. A* **2018**, *49*, 6553–6560. [CrossRef]
13. Prokoshkin, S.; Pustov, Y.; Zhukova, Y.; Kadirov, P.; Dubinskiy, S.; Sheremetyev, V.; Karavaeva, M. Effect of Thermomechanical Treatment on Functional Properties of Biodegradable Fe-30Mn-5Si Shape Memory Alloy. *Metall. Mater. Trans. A* **2021**, *52*, 2024–2032. [CrossRef]
14. Koumya, Y.; Ait Salam, Y.; Khadiri, M.E.; Benzakour, J.; Romane, A.; Abouelfida, A.; Benyaich, A. Pitting corrosion behavior of SS-316L in simulated body fluid and electrochemically assisted deposition of hydroxyapatite coating. *Chem. Pap.* **2021**, *75*, 2667–2682. [CrossRef]
15. Trincă, L.C.; Burtan, L.; Mareci, D.; Fernández-Pérez, B.M.; Stoleriu, I.; Stanciu, T.; Stanciu, S.; Solcan, C.; Izquierdo, J.; Souto, R.M. Evaluation of in vitro corrosion resistance and in vivo osseointegration properties of a FeMnSiCa alloy as potential degradable implant biomaterial. *Mater. Sci. Eng. C* **2021**, *118*, 111436. [CrossRef] [PubMed]
16. Tchana Nkonta, D.V.; Simescu-Lazar, F.; Drevet, R.; Aaboubi, O.; Fauré, J.; Retraint, D.; Benhayoune, H. Influence of the surface mechanical attrition treatment (SMAT) on the corrosion behavior of Co28Cr6Mo alloy in Ringer's solution. *J. Solid State Electrochem.* **2018**, *22*, 1091–1098. [CrossRef]
17. Chen, Y.; Li, Y.; Kurosu, S.; Yamanaka, K.; Tang, N.; Koizumi, Y.; Chiba, A. Effects of sigma phase and carbide on the wear behavior of CoCrMo alloys in Hanks' solution. *Wear* **2014**, *310*, 51–62. [CrossRef]
18. Tchana Nkonta, D.V.; Drevet, R.; Fauré, J.; Benhayoune, H. Effect of surface mechanical attrition treatment on the microstructure of cobalt–chromium–molybdenum biomedical alloy. *Microsc. Res. Tech.* **2021**, *84*, 238–245. [CrossRef]
19. AlMangour, B.; Luqman, M.; Grzesiak, D.; Al-Harbi, H.; Ijaz, F. Effect of processing parameters on the microstructure and mechanical properties of Co–Cr–Mo alloy fabricated by selective laser melting. *Mater. Sci. Eng. A* **2020**, *792*, 139456. [CrossRef]
20. Yamanaka, K.; Mori, M.; Kurosu, S.; Matsumoto, H.; Chiba, A. Ultrafine grain refinement of biomedical Co-29Cr-6Mo alloy during conventional hot-compression deformation. *Metall. Mater. Trans. A* **2009**, *40*, 1980–1994. [CrossRef]
21. İbrahim Coşkun, M.; Karahan, İ.H.; Yücel, Y.; Golden, T.D. Optimization of electrochemical step deposition for bioceramic hydroxyapatite coatings on CoCrMo implants. *Surf. Coat. Technol.* **2016**, *301*, 42–53. [CrossRef]
22. Coşkun, M.I.; Karahan, I.H.; Yücel, Y. Optimized electrodeposition concentrations for hydroxyapatite coatings on CoCrMo biomedical alloys by computational techniques. *Electrochim. Acta* **2014**, *150*, 46–54. [CrossRef]
23. Ghasemi-Mobarakeh, L.; Kolahreez, D.; Ramakrishna, S.; Williams, D. Key terminology in biomaterials and biocompatibility. *Curr. Opin. Biomed. Eng.* **2019**, *10*, 45–50. [CrossRef]
24. Williams, D. Revisiting the definition of biocompatibility. *Med. Device Technol.* **2003**, *14*, 10–13. [PubMed]
25. Williams, D.F. On the mechanisms of biocompatibility. *Biomaterials* **2008**, *29*, 2941–2953. [CrossRef] [PubMed]

26. Paital, S.R.; Dahotre, N.B. Calcium phosphate coatings for bio-implant applications: Materials, performance factors, and methodologies. *Mater. Sci. Eng. R* **2009**, *66*, 1–70. [CrossRef]
27. Dorozhkin, S.V. Calcium orthophosphate deposits: Preparation, properties and biomedical applications. *Mater. Sci. Eng. C* **2015**, *55*, 272–326. [CrossRef] [PubMed]
28. Dorozhkin, S.V. Bioceramics of calcium orthophosphates. *Biomaterials* **2010**, *31*, 1465–1485. [CrossRef]
29. LeGeros, R.Z. Calcium phosphate-based osteoinductive materials. *Chem. Rev.* **2008**, *108*, 4742–4753. [CrossRef]
30. Surmenev, R.A.; Surmeneva, M.A.; Ivanova, A.A. Significance of calcium phosphate coatings for the enhancement of new bone osteogenesis—A review. *Acta Biomater.* **2014**, *10*, 557–579. [CrossRef]
31. Vallet-Regí, M.; González-Calbet, J.M. Calcium phosphates as substitution of bone tissues. *Prog. Solid State Chem.* **2004**, *32*, 1–31. [CrossRef]
32. Fiume, E.; Magnaterra, G.; Rahdar, A.; Verné, E.; Baino, F. Hydroxyapatite for Biomedical Applications: A Short Overview. *Ceramics* **2021**, *4*, 542–563. [CrossRef]
33. Williams, D.F. Biocompatibility pathways and mechanisms for bioactive materials: The bioactivity zone. *Bioact. Mater.* **2022**, *10*, 306–322. [CrossRef] [PubMed]
34. Williams, D.F. On the nature of biomaterials. *Biomaterials* **2009**, *30*, 5897–5909. [CrossRef] [PubMed]
35. Cao, W.; Hench, L.L. Bioactive materials. *Ceram. Int.* **1996**, *22*, 493–507. [CrossRef]
36. Hench, L.L. Bioceramics. *J. Am. Ceram. Soc.* **1998**, *81*, 1705–1728. [CrossRef]
37. Albrektsson, T.; Johansson, C. Osteoinduction, osteoconduction and osseointegration. *Eur. Spine J.* **2001**, *10*, S96–S101. [CrossRef] [PubMed]
38. Heimann, R.B. Thermal spraying of biomaterials. *Surf. Coat. Technol.* **2006**, *201*, 2012–2019. [CrossRef]
39. Heimann, R.B. On the self-affine fractal geometry of plasma-sprayed surfaces. *J. Therm. Spray Technol.* **2011**, *20*, 898–908. [CrossRef]
40. Heimann, R.B. Structural Changes of Hydroxylapatite during Plasma Spraying: Raman and NMR Spectroscopy Results. *Coatings* **2021**, *11*, 987. [CrossRef]
41. Chambard, M.; Remache, D.; Balcaen, Y.; Dalverny, O.; Alexis, J.; Siadous, R.; Bareille, R.; Catros, S.; Fort, P.; Grossin, D.; et al. Effect of silver and strontium incorporation route on hydroxyapatite coatings elaborated by rf-SPS. *Materialia* **2020**, *12*, 100809. [CrossRef]
42. Chambard, M.; Marsan, O.; Charvillat, C.; Grossin, D.; Fort, P.; Rey, C.; Gitzhofer, F.; Bertrand, G. Effect of the deposition route on the microstructure of plasma-sprayed hydroxyapatite coatings. *Surf. Coat. Technol.* **2019**, *371*, 68–77. [CrossRef]
43. Heimann, R.B. Plasma-Sprayed Hydroxylapatite-Based Coatings: Chemical, Mechanical, Microstructural, and Biomedical Properties. *J. Therm. Spray Technol.* **2016**, *25*, 827–850. [CrossRef]
44. Heimann, R.B. Functional plasma-sprayed hydroxylapatite coatings for medical application: Clinical performance requirements and key property enhancement. *J. Vac. Sci. Technol. A* **2021**, *39*, 050801. [CrossRef]
45. Gross, K.A.; Walsh, W.; Swarts, E. Analysis of retrieved hydroxyapatite-coated hip prostheses. *J. Therm. Spray Technol.* **2004**, *13*, 190–199. [CrossRef]
46. Chernozem, R.V.; Surmeneva, M.A.; Krause, B.; Baumbach, T.; Ignatov, V.P.; Tyurin, A.I.; Loza, K.; Epple, M.; Surmenev, R.A. Hybrid biocomposites based on titania nanotubes and a hydroxyapatite coating deposited by RF-magnetron sputtering: Surface topography, structure, and mechanical properties. *Appl. Surf. Sci.* **2017**, *426*, 229–237. [CrossRef]
47. Surmenev, R.A.; Ivanova, A.A.; Epple, M.; Pichugin, V.F.; Surmeneva, M.A. Physical principles of radio-frequency magnetron sputter deposition of calcium-phosphate-based coating with tailored properties. *Surf. Coat. Technol.* **2021**, *413*, 127098. [CrossRef]
48. Safavi, M.S.; Surmeneva, M.A.; Surmenev, R.A.; Khalil-Allafi, J. RF-magnetron sputter deposited hydroxyapatite-based composite & multilayer coatings: A systematic review from mechanical, corrosion, and biological points of view. *Ceram. Int.* **2021**, *47*, 3031–3053. [CrossRef]
49. Surmeneva, M.A.; Ivanova, A.A.; Tian, Q.; Pittman, R.; Jiang, W.; Lin, J.; Liu, H.H.; Surmenev, R.A. Bone marrow derived mesenchymal stem cell response to the RF magnetron sputter deposited hydroxyapatite coating on AZ91 magnesium alloy. *Mater. Chem. Phys.* **2019**, *221*, 89–98. [CrossRef]
50. Ivanova, A.A.; Surmeneva, M.A.; Tyurin, A.I.; Surmenev, R.A. Correlation between structural and mechanical properties of RF magnetron sputter deposited hydroxyapatite coating. *Mater. Charact.* **2018**, *142*, 261–269. [CrossRef]
51. Nelea, V.; Morosanu, C.; Iliescu, M.; Mihailescu, I.N. Microstructure and mechanical properties of hydroxyapatite thin films grown by RF magnetron sputtering. *Surf. Coat. Technol.* **2003**, *173*, 315–322. [CrossRef]
52. Garcia-Sanz, F.J.; Mayor, M.B.; Arias, J.L.; Pou, J.; Leon, B.; Perez-Amor, M. Hydroxyapatite coatings: A comparative study between plasma-spray and pulsed laser deposition techniques. *J. Mater. Sci.–Mater. Med.* **1997**, *8*, 861–865. [CrossRef] [PubMed]
53. Koch, C.F.; Johnson, S.; Kumar, D.; Jelinek, M.; Chrisey, D.B.; Doraiswamy, A.; Jin, C.; Narayan, R.J.; Mihailescu, I.N. Pulsed laser deposition of hydroxyapatite thin films. *Mater. Sci. Eng. C* **2007**, *27*, 484–494. [CrossRef]
54. Popescu-Pelin, G.; Sima, F.; Sima, L.E.; Mihailescu, C.N.; Luculescu, C.; Iordache, I.; Socol, M.; Socol, G.; Mihailescu, I.N. Hydroxyapatite thin films grown by pulsed laser deposition and matrix assisted pulsed laser evaporation: Comparative study. *Appl. Surf. Sci.* **2017**, *418 Pt 8*, 580–588. [CrossRef]
55. Azzouz, I.; Faure, J.; Khlifi, K.; Cheikh Larbi, A.; Benhayoune, H. Electrophoretic Deposition of 45S5 Bioglass® Coatings on the Ti6Al4V Prosthetic Alloy with Improved Mechanical Properties. *Coatings* **2020**, *10*, 1192. [CrossRef]

56. Akhtar, M.A.; Hadzhieva, Z.; Dlouhý, I.; Boccaccini, A.R. Electrophoretic Deposition and Characterization of Functional Coatings Based on an Antibacterial Gallium (III)-Chitosan Complex. *Coatings* **2020**, *10*, 483. [CrossRef]
57. Virk, R.S.; Rehman, M.A.U.; Munawar, M.A.; Schubert, D.W.; Goldmann, W.H.; Dusza, J.; Boccaccini, A.R. Curcumin-Containing Orthopedic Implant Coatings Deposited on Poly-Ether-Ether-Ketone/Bioactive Glass/Hexagonal Boron Nitride Layers by Electrophoretic Deposition. *Coatings* **2019**, *9*, 572. [CrossRef]
58. Faure, J.; Drevet, R.; Ben Jaber, N.; Potiron, S.; Demangel, C.; Retraint, D.; Benhayoune, H. Electrophoretic Deposition of Hydroxyapatite and 58S Bioactive Glass coatings on the Ti6Al4V alloy subjected to Surface Mechanical Attrition Treatment. *Key Eng. Mater.* **2015**, *654*, 149–153. [CrossRef]
59. Drevet, R.; Ben Jaber, N.; Fauré, J.; Tara, A.; Ben Cheikh Larbi, A.; Benhayoune, H. Electrophoretic deposition (EPD) of Nano-hydroxyapatite coatings with improved mechanical properties on prosthetic Ti6Al4V substrates. *Surf. Coat. Technol.* **2016**, *301*, 94–99. [CrossRef]
60. Bartmański, M.; Pawłowski, Ł.; Strugała, G.; Mielewczyk-Gryń, A.; Zieliński, A. Properties of nanohydroxyapatite coatings doped with nanocopper, obtained by electrophoretic deposition on Ti13Zr13Nb alloy. *Materials* **2019**, *12*, 3741. [CrossRef]
61. Bartmanski, M.; Cieslik, B.; Glodowska, J.; Kalka, P.; Pawlowski, L.; Pieper, M.; Zielinski, A. Electrophoretic deposition (EPD) of nanohydroxyapatite—Nanosilver coatings on Ti13Zr13Nb alloy. *Ceram. Int.* **2017**, *43*, 11820–11829. [CrossRef]
62. Ozhukil Kollath, V.; Chen, Q.; Closset, R.; Luyten, L.; Traina, K.; Mullens, S.; Boccaccini, A.R.; Cloots, R. AC vs. DC electrophoretic deposition of hydroxyapatite on titanium. *J. Eur. Ceram. Soc.* **2013**, *33*, 2715–2721. [CrossRef]
63. Corni, I.; Ryan, M.P.; Boccaccini, A.R. Electrophoretic deposition: From traditional ceramics to nanotechnology. *J. Eur. Ceram. Soc.* **2008**, *28*, 1353–1367. [CrossRef]
64. Boccaccini, A.R.; Zhitomirsky, I. Application of electrophoretic and electrolytic deposition techniques in ceramics processing. *Curr. Opin. Solid State Mater. Sci.* **2002**, *6*, 251–260. [CrossRef]
65. Kwok, C.T.; Wong, P.K.; Cheng, F.T.; Man, H.C. Characterization and corrosion behavior of hydroxyapatite coatings on Ti6Al4V fabricated by electrophoretic deposition. *Appl. Surf. Sci.* **2009**, *255*, 6736–6744. [CrossRef]
66. Boccaccini, A.R.; Keim, S.; Ma, R.; Li, Y.; Zhitomirsky, I. Electrophoretic deposition of biomaterials. *J. R. Soc. Interface* **2010**, *7*, S581–S613. [CrossRef]
67. Eliaz, N.; Sridhar, T.M.; Mudali, U.K.; Raj, B. Electrochemical and electrophoretic deposition of hydroxyapatite for orthopaedic applications. *Surf. Eng.* **2005**, *21*, 238–242. [CrossRef]
68. Eliaz, N.; Eliyahu, M. Electrochemical processes of nucleation and growth of hydroxyapatite on titanium supported by real-time electrochemical atomic force microscopy. *J. Biomed. Mater. Res. A* **2007**, *80*, 621–634. [CrossRef]
69. Eliaz, N.; Sridhar, T.M. Electrocrystallization of hydroxyapatite and its dependence on solution conditions. *Cryst. Growth Des.* **2008**, *8*, 3965–3977. [CrossRef]
70. Metoki, N.; Leifenberg-Kuznits, L.; Kopelovich, W.; Burstein, L.; Gozin, M.; Eliaz, N. Hydroxyapatite coatings electrodeposited at near-physiological conditions. *Mater. Lett.* **2014**, *119*, 24–27. [CrossRef]
71. Eliaz, N.; Metoki, N. Calcium phosphate bioceramics: A review of their history, structure, properties, coating technologies and biomedical applications. *Materials* **2017**, *10*, 334. [CrossRef]
72. Benhayoune, H.; Drevet, R.; Fauré, J.; Potiron, S.; Gloriant, T.; Oudadesse, H.; Laurent-Maquin, D. Elaboration of Monophasic and Biphasic Calcium Phosphate Coatings on Ti6Al4V Substrate by Pulsed Electrodeposition Current. *Adv. Eng. Mater.* **2010**, *12*, B192–B199. [CrossRef]
73. Drevet, R.; Benhayoune, H.; Wortham, L.; Potiron, S.; Douglade, J.; Laurent-Maquin, D. Effects of Pulsed Current and H_2O_2 Amount on the Composition of Electrodeposited Calcium Phosphate Coatings. *Mater. Charact.* **2010**, *61*, 786–795. [CrossRef]
74. Drevet, R.; Velard, F.; Potiron, S.; Laurent-Maquin, D.; Benhayoune, H. In vitro dissolution and corrosion study of calcium phosphate coatings elaborated by pulsed electrodeposition current on Ti6Al4V substrate. *J. Mater. Sci.–Mater. Med.* **2011**, *22*, 753–761. [CrossRef] [PubMed]
75. Drevet, R.; Aaboubi, O.; Benhayoune, H. In vitro corrosion behavior of electrodeposited calcium phosphate coatings on Ti6Al4V Substrates. *J. Solid State Electrochem.* **2012**, *16*, 3069–3077. [CrossRef]
76. Drevet, R.; Lemelle, A.; Untereiner, V.; Manfait, M.; Sockalingum, G.D.; Benhayoune, H. Morphological modifications of electrodeposited calcium phosphate coatings under amino acids effect. *Appl. Surf. Sci.* **2013**, *268*, 343–348. [CrossRef]
77. Drevet, R.; Viteaux, A.; Maurin, J.C.; Benhayoune, H. Human osteoblast-like cells response to pulsed electrodeposited calcium phosphate coatings. *RSC Adv.* **2013**, *3*, 11148–11154. [CrossRef]
78. Zielinski, A.; Bartmanski, M. Electrodeposited biocoatings, their properties and fabrication technologies: A review. *Coatings* **2020**, *10*, 782. [CrossRef]
79. Olivier, F.; Picard, Q.; Delpeux-Ouldriane, S.; Chancolon, J.; Warmont, F.; Sarou-Kanian, V.; Fayon, F.; Bonnamy, S. Influence of electrochemical parameters on the characteristics of sono-electrodeposited calcium phosphate-coated carbon fiber cloth. *Surf. Coat. Technol.* **2020**, *389*, 125507. [CrossRef]
80. Olivier, F.; Rochet, N.; Delpeux-Ouldriane, S.; Chancolon, J.; Sarou-Kanian, V.; Fayon, F.; Bonnamy, S. Strontium incorporation into biomimetic carbonated calcium-deficient hydroxyapatite coated carbon cloth: Biocompatibility with human primary osteoblasts. *Mater. Sci. Eng. C* **2020**, *116*, 111192. [CrossRef]

81. Vidal, E.; Buxadera-Palomero, J.; Pierre, C.; Manero, J.M.; Ginebra, M.P.; Cazalbou, S.; Combes, C.; Rupérez, E.; Rodríguez, D. Single-step pulsed electrodeposition of calcium phosphate coatings on titanium for drug delivery. *Surf. Coat. Technol.* **2019**, *358*, 266–275. [CrossRef]
82. Jimenez-Garcia, F.N.; Giraldo-Torres, L.R.; Restrepo-Parra, E. Electrochemically deposited calcium phosphate coatings using a potentiostat of in-house design and implementation. *Mater. Res.* **2021**, *25*, e20210098. [CrossRef]
83. Valenti, L.E.; Bonnet, L.V.; Galiano, M.R.; Giacomelli, C.E. A simple strategy to prepare hybrid coating on titanium (Ti6Al4V). *Surf. Coat. Technol.* **2022**, *431*, 128017. [CrossRef]
84. Vidal, E.; Guillem-Marti, J.; Ginebra, M.-P.; Combes, C.; Rupérez, E.; Rodriguez, D. Multifunctional homogeneous calcium phosphate coatings: Toward antibacterial and cell adhesive titanium scaffolds. *Surf. Coat. Technol.* **2021**, *405*, 126557. [CrossRef]
85. Drevet, R.; Benhayoune, H. Electrochemical Deposition of Calcium Phosphate Coatings on a Prosthetic Titanium Alloy Substrate. In *Calcium Phosphate: Structure, Synthesis, Properties and Applications*; Heimann, R.B., Ed.; Nova Science Publishers, Inc.: Hauppauge, NY, USA, 2012; pp. 231–252. ISBN 978-162257299-1.
86. Safavi, M.S.; Walsh, F.C.; Surmeneva, M.A.; Surmenev, R.A.; Khalil-Allafi, J. Electrodeposited hydroxyapatite-based biocoatings: Recent progress and future challenges. *Coatings* **2021**, *11*, 110. [CrossRef]
87. Kuo, M.C.; Yen, S.K. The process of electrochemical deposited hydroxyapatite coatings on biomedical titanium at room temperature. *Mater. Sci. Eng. C* **2002**, *20*, 153–160. [CrossRef]
88. Lopez-Heredia, M.A.; Weiss, P.; Layrolle, P. An electrodeposition method of calcium phosphate coatings on titanium alloy. *J. Mater. Sci.–Mater. Med.* **2007**, *18*, 381–390. [CrossRef]
89. Abdel-Aal, E.A.; Dietrich, D.; Steinhaeuser, S.; Wielage, B. Electrocrystallization of nanocrystallite calcium phosphate coatings on titanium substrate at different current densities. *Surf. Coat. Technol.* **2008**, *202*, 5895–5900. [CrossRef]
90. Ban, S.; Maruno, S. Morphology and microstructure of electrochemically deposited calcium phosphates in a modified simulated body fluid. *Biomaterials* **1998**, *19*, 1245–1253. [CrossRef]
91. Strąkowska, P.; Beutner, R.; Gnyba, M.; Zielinski, A.; Scharnweber, D. Electrochemically assisted deposition of hydroxyapatite on Ti6Al4V substrates covered by CVD diamond films—Coating characterization and first cell biological results. *Mater. Sci. Eng. C* **2016**, *59*, 624–635. [CrossRef]
92. Rößler, S.; Sewing, A.; Stölzel, M.; Born, R.; Scharnweber, D.; Dard, M.; Worch,, H. Electrochemically assisted deposition of thin calcium phosphate coatings at near-physiological pH and temperature. *J. Biomed. Mater. Res. A* **2003**, *64*, 655–663. [CrossRef]
93. Shirkhanzadeh, M. Bioactive calcium phosphate coatings prepared by electrodeposition. *J. Mater. Sci. Lett.* **1991**, *10*, 1415–1417. [CrossRef]
94. Shirkhanzadeh, M. Direct formation of nanophase hydroxyapatite on cathodically polarized electrodes. *J. Mater. Sci.–Mater. Med.* **1998**, *9*, 67–72. [CrossRef] [PubMed]
95. Shirkhanzadeh, M. Calcium phosphate coatings prepared by electrocrystallization from aqueous electrolytes. *J. Mater. Sci.–Mater. Med.* **1995**, *6*, 90–93. [CrossRef]
96. Narayanan, R.; Kwon, T.Y.; Kim, K.H. Direct nanocrystalline hydroxyapatite formation on titanium from ultrasonated electrochemical bath at physiological pH. *Mater. Sci. Eng. C* **2008**, *28*, 1265–1270. [CrossRef]
97. Therese, G.H.A.; Kamath, P.V. Electrochemical synthesis of metal oxides and hydroxides. *Chem. Mater.* **2000**, *12*, 1195–1204. [CrossRef]
98. Gao, A.; Hang, R.; Bai, L.; Tang, B.; Chu, P.K. Electrochemical surface engineering of titanium-based alloys for biomedical application. *Electrochim. Acta* **2018**, *271*, 699–718. [CrossRef]
99. Available online: https://en.wikipedia.org/wiki/Phosphate (accessed on 23 March 2022).
100. Redepenning, J.; McIsaac, J.P. Electrocrystallization of Brushite Coatings on Prosthetic Alloys. *Chem. Mater.* **1990**, *2*, 625–627. [CrossRef]
101. Da Rocha, D.N.; Da Silva, M.H.P.; De Campos, J.B.; Santana Blazutti Marçal, R.L.; Mijares, D.Q.; Coelho, P.G.; Cruz, L.R. Kinetics of conversion of brushite coatings to hydroxyapatite in alkaline solution. *J. Mater. Res. Technol.* **2018**, *7*, 479–486. [CrossRef]
102. Abdel-Aal, E.A.; El-Sayed, D.; Shoeib, M.; Kandil, A.T. Enhancing coating of brushite/hydroxyapatite layer on titanium alloy implant surface with additives. *Appl. Surf. Sci.* **2013**, *285*, 136–143. [CrossRef]
103. Lin, S.; LeGeros, R.Z.; LeGeros, J.P. Adherent octacalcium phosphate coating on titanium alloy using modulated electrochemical deposition method. *J. Biomed. Mater. Res. A* **2003**, *66*, 819–828. [CrossRef]
104. Lu, X.; Leng, Y.; Zhang, Q. Electrochemical deposition of octacalcium phosphate micro-fiber/chitosan composite coatings on titanium substrates. *Surf. Coat. Technol.* **2008**, *202*, 3142–3147. [CrossRef]
105. Yang, Y.; Wang, H.; Yan, F.Y.; Qi, Y.; Lai, Y.K.; Zeng, D.M.; Chen, G.; Zhang, K.Q. Bioinspired Porous Octacalcium Phosphate/Silk Fibroin Composite Coating Materials Prepared by Electrochemical Deposition. *ACS Appl. Mater. Interfaces* **2015**, *7*, 5634–5642. [CrossRef] [PubMed]
106. Dumelie, N.; Benhayoune, H.; Richard, D.; Laurent-Maquin, D.; Balossier, G. In vitro precipitation of electrodeposited calcium-deficient hydroxyapatite coatings on Ti6Al4V substrate. *Mater. Charact.* **2008**, *59*, 129–133. [CrossRef]
107. Wang, H.; Zhu, Z.; Wang, L.; Feng, Y.; Ma, X.; Guan, S. Formation mechanism of Ca-deficient hydroxyapatite coating on Mg–Zn–Ca alloy for orthopaedic implant. *Appl. Surf. Sci.* **2014**, *307*, 92–100. [CrossRef]
108. Wang, H.; Guan, S.; Wang, Y.; Liu, H.; Wang, H.; Wang, L.; Ren, C.; Zhu, S.; Chen, K. In vivo degradation behavior of Ca-deficient hydroxyapatite coated Mg–Zn–Ca alloy for bone implant application. *Colloids Surf. B* **2011**, *88*, 254–259. [CrossRef]

109. Drevet, R.; Fauré, J.; Sayen, S.; Marle-Spiess, M.; El Btaouri, H.; Benhayoune, H. Electrodeposition of biphasic calcium phosphate coatings with improved dissolution properties. *Mater. Chem. Phys.* **2019**, *236*, 121797. [CrossRef]
110. Metoki, N.; Rosa, C.M.R.; Zanin, H.; Marciano, F.R.; Eliaz, N.; Lobo, A.O. Electrodeposition and biomineralization of nano-β-tricalcium phosphate on graphenated carbon nanotubes. *Surf. Coat. Technol.* **2016**, *297*, 51–57. [CrossRef]
111. Ben Jaber, N.; Drevet, R.; Fauré, J.; Demangel, C.; Potiron, S.; Tara, A.; Ben Cheikh Larbi, A.; Benhayoune, H. A new process for the thermal treatment of calcium phosphate coatings electrodeposited on Ti6Al4V substrate. *Adv. Eng. Mater.* **2015**, *17*, 1608–1615. [CrossRef]
112. Drouet, C. Apatite formation: Why it may not work as planned, and how to conclusively identify apatite compounds. *BioMed Res. Int.* **2013**, *2013*, 490946. [CrossRef]
113. Antonakos, A.; Liarokapis, E.; Leventouri, T. Micro-Raman and FTIR studies of synthetic and natural apatites. *Biomaterials* **2007**, *28*, 3043–3054. [CrossRef]
114. Bohner, M.; Le Gars Santoni, B.; Döbelin, N. β-tricalcium phosphate for bone substitution: Synthesis and properties. *Acta Biomater.* **2020**, *113*, 23–41. [CrossRef] [PubMed]
115. Chaair, H.; Labjar, H.; Britel, O. Synthesis of β-tricalcium phosphate. *Morphologie* **2017**, *101*, 120–124. [CrossRef] [PubMed]
116. Zhitomirsky, I. Electrophoretic and electrolytic deposition of ceramic coatings on carbon fibers. *J. Eur. Ceram. Soc.* **1998**, *18*, 849–856. [CrossRef]
117. Zhitomirsky, I. Cathodic electrodeposition of ceramic and organoceramic materials. Fundamental aspects. *Adv. Colloid Interface Sci.* **2002**, *97*, 279–317. [CrossRef]
118. Tsai, W.L.; Hsu, P.C.; Hwu, Y.; Chen, C.H.; Chang, L.W.; Je, J.H.; Lin, H.M.; Groso, A.; Margaritondo, G. Electrochemistry: Building on bubbles in metal electrodeposition. *Nature* **2002**, *417*, 139. [CrossRef] [PubMed]
119. Azem, F.A.; Delice, T.K.; Ungan, G.; Cakir, A. Investigation of duty cycle effect on corrosion properties of electrodeposited calcium phosphate coatings. *Mater. Sci. Eng. C* **2016**, *68*, 681–686. [CrossRef] [PubMed]
120. Gopi, D.; Karthika, A.; Nithiya, S.; Kavitha, L. In vitro biological performance of minerals substituted hydroxyapatite coating by pulsed electrodeposition method. *Mater. Chem. Phys.* **2014**, *144*, 75–85. [CrossRef]
121. Furko, M.; Balázsi, C. Calcium phosphate based bioactive ceramic layers on implant materials preparation, properties, and biological performance. *Coatings* **2020**, *10*, 823. [CrossRef]
122. Dumelié, N.; Benhayoune, H.; Rousse-Bertrand, C.; Bouthors, S.; Perchet, A.; Wortham, L.; Douglade, J.; Laurent-Maquin, D.; Balossier, G. Characterization of electrodeposited calcium phosphate coatings by complementary scanning electron microscopy and scanning-transmission electron microscopy associated to X-ray microanalysis. *Thin Solid Films* **2005**, *492*, 131–139. [CrossRef]
123. Zhitomirsky, I. Electrolytic deposition of oxide films in the presence of hydrogen peroxide. *J. Eur. Ceram. Soc.* **1999**, *19*, 2581–2587. [CrossRef]
124. Ducheyne, P.; Qiu, Q. Bioactive ceramics: The effect of surface reactivity on bone formation and bone cell function. *Biomaterials* **1999**, *20*, 2287–2303. [CrossRef]
125. Lee, W.K.; Lee, S.M.; Kim, H.M. Effect of surface morphology of calcium phosphate on osteoblast-like HOS cell responses. *J. Ind. Eng. Chem.* **2009**, *15*, 677–682. [CrossRef]
126. Iwamoto, T.; Hieda, Y.; Kogai, Y. Effect of hydroxyapatite surface morphology on cell adhesion. *Mater. Sci. Eng. C* **2016**, *69*, 1263–1267. [CrossRef] [PubMed]
127. Chen, S.; Guo, Y.; Liu, R.; Wu, S.; Fang, J.; Huang, B.; Li, Z.; Chen, Z.; Chen, Z. Tuning surface properties of bone biomaterials to manipulate osteoblastic cell adhesion and the signaling pathways for the enhancement of early osseointegration. *Colloids Surf. B* **2018**, *164*, 58–69. [CrossRef] [PubMed]
128. Khlusov, I.A.; Dekhtyar, Y.; Sharkeev, Y.P.; Pichugin, V.F.; Khlusova, M.Y.; Polyaka, N.; Tyulkin, F.; Vendinya, V.; Legostaeva, E.V.; Litvinova, L.S.; et al. Nanoscale electrical potential and roughness of a calcium phosphate surface promotes the osteogenic phenotype of stromal cells. *Materials* **2018**, *11*, 978. [CrossRef] [PubMed]
129. Deligianni, D.D.; Katsala, N.D.; Koutsoukos, P.G.; Missirlis, Y.F. Effect of surface roughness of hydroxyapatite on human bone marrow cell adhesion, proliferation, differentiation and detachment strength. *Biomaterials* **2000**, *22*, 87–96. [CrossRef]
130. Cairns, M.L.; Meenan, B.J.; Burke, G.A.; Boyd, A.R. Influence of surface topography on osteoblast response to fibronectin coated calcium phosphate thin films. *Colloids Surf. B* **2010**, *78*, 283–290. [CrossRef]
131. Anselme, K.; Bigerelle, M. On the Relation Between Surface Roughness of Metallic Substrates and Adhesion of Human Primary Bone Cells. *Scanning* **2014**, *36*, 11–20. [CrossRef]
132. Giljean, S.; Bigerelle, M.; Anselme, K. Roughness Statistical Influence on Cell Adhesion Using Profilometry and Multiscale Analysis. *Scanning* **2014**, *36*, 2–10. [CrossRef]
133. Fornell, J.; Feng, Y.P.; Pellicer, E.; Suriñach, S.; Baró, M.D.; Sort, J. Mechanical behaviour of brushite and hydroxyapatite coatings electrodeposited on newly developed FeMnSiPd alloys. *J. Alloys Compd.* **2017**, *729*, 231–239. [CrossRef]
134. Raynaud, S.; Champion, E.; Bernache-Assollant, D. Calcium phosphate apatites with variable Ca/P atomic ratio II. Calcination and sintering. *Biomaterials* **2002**, *23*, 1073–1080. [CrossRef]
135. Destainville, A.; Champion, E.; Bernache-Assollant, D.; Laborde, E. Synthesis, characterization and thermal behavior of apatitic tricalcium phosphate. *Mater. Chem. Phys.* **2003**, *80*, 269–277. [CrossRef]
136. Drevet, R.; Fauré, J.; Benhayoune, H. Structural and morphological study of electrodeposited calcium phosphate materials submitted to thermal treatment. *Mater. Lett.* **2017**, *209*, 27–31. [CrossRef]

137. *ISO 13779-4*; Implants for Surgery—Hydroxyapatite—Part 4: Determination of Coating Adhesion Strength. ISO: Geneva, Switzerland, 2018.
138. Drevet, R.; Fauré, J.; Benhayoune, H. Thermal Treatment Optimization of Electrodeposited Hydroxyapatite Coatings on Ti6Al4V Substrate. *Adv. Eng. Mater.* **2012**, *14*, 377–382. [CrossRef]
139. Furko, M.; Balázsi, C. Morphological, chemical, and biological investigation of ionic substituted, pulse current deposited calcium phosphate coatings. *Materials* **2020**, *13*, 4690. [CrossRef]
140. Ungureanu, E.; Vranceanu, D.M.; Vladescu, A.; Parau, A.C.; Tarcolea, M.; Cotrut, C.M. Effect of doping element and electrolyte's pH on the properties of hydroxyapatite coatings obtained by pulsed galvanostatic technique. *Coatings* **2021**, *11*, 1522. [CrossRef]
141. Panda, S.; Biswas, C.K.; Paul, S. A comprehensive review on the preparation and application of calcium hydroxyapatite: A special focus on atomic doping methods for bone tissue engineering. *Ceram. Int.* **2021**, *47*, 28122–28144. [CrossRef]
142. Schatkoski, V.M.; Larissa do Amaral Montanheiro, T.; Canuto de Menezes, B.R.; Pereira, R.M.; Rodrigues, K.F.; Ribas, R.G.; Morais da Silva, D.; Thim, G.P. Current advances concerning the most cited metal ions doped bioceramics and silicate-based bioactive glasses for bone tissue engineering. *Ceram. Int.* **2021**, *47*, 2999–3012. [CrossRef]
143. Boanini, E.; Gazzano, M.; Bigi, A. Ionic substitutions in calcium phosphates synthesized at low temperature. *Acta Biomater.* **2010**, *6*, 1882–1894. [CrossRef] [PubMed]
144. Bigi, A.; Boanini, E.; Gazzano, M. Ion Substitution in Biological and Synthetic Apatites. *Biominer. Biomater. Fundam. Appl.* **2016**, 235–266. [CrossRef]
145. Wang, W.; Yeung, K.W.K. Bone grafts and biomaterials substitutes for bone defect repair: A review. *Bioact. Mater.* **2017**, *2*, 224–247. [CrossRef] [PubMed]
146. Arcos, D.; Vallet-Regi, M. Substituted hydroxyapatite coatings of bone implants. *J. Mater. Chem. B* **2020**, *8*, 1781–1800. [CrossRef] [PubMed]
147. Ratnayake, J.T.B.; Mucalo, M.; Dias, G.J. Substituted hydroxyapatites for bone regeneration: A review of current trends. *J. Biomed. Mater. Res. B* **2017**, *105B*, 1285–1299. [CrossRef] [PubMed]
148. Tang, C.-M.; Fan, F.-Y.; Ke, Y.-C.; Lin, W.-C. Effects of electrode plate annealing treatment and the addition of hydrogen peroxide on improving the degradation of cobalt hydroxyapatite for bone repair. *Mater. Chem. Phys.* **2021**, *259*, 123962. [CrossRef]
149. Drevet, R.; Zhukova, Y.; Dubinskiy, S.; Kazakbiev, A.; Naumenko, V.; Abakumov, M.; Fauré, J.; Benhayoune, H.; Prokoshkin, S. Electrodeposition of cobalt-substituted calcium phosphate coatings on Ti22Nb6Zr alloy for bone implant applications. *J. Alloys Compd.* **2019**, *793*, 576–582. [CrossRef]
150. Grass, G.; Rensing, C.; Solioz, M. Metallic copper as an antimicrobial surface. *Appl. Environ. Microbiol.* **2011**, *77*, 1541–1547. [CrossRef]
151. Hajipour, M.J.; Fromm, K.M.; Ashkarran, A.A.; Jimenez de Aberasturi, D.; Ruiz de Larramendi, I.; Rojo, T.; Serpooshan, V.; Parak, W.J.; Mahmoudi, M. Antibacterial properties of nanoparticles. *Trends Biotechnol.* **2012**, *30*, 499–511. [CrossRef]
152. Wolf-Brandstetter, C.; Oswald, S.; Bierbaum, S.; Wiesmann, H.-P.; Scharnweber, D. Influence of pulse ratio on codeposition of copper species with calcium phosphate coatings on titanium by means of electrochemically assisted deposition. *J. Biomed. Mater. Res. B* **2014**, *102*, 160–172. [CrossRef]
153. Bakin, B.; Koc Delice, T.; Tiric, U.; Birlik, I.; Ak Azem, F. Bioactivity and corrosion properties of magnesium-substituted CaP coatings produced via electrochemical deposition. *Surf. Coat. Technol.* **2016**, *301*, 29–35. [CrossRef]
154. Cacciotti, I.; Bianco, A.; Lombardi, M.; Montanaro, L. Mg-substituted hydroxyapatite nanopowders: Synthesis, thermal stability and sintering behaviour. *J. Eur. Ceram. Soc.* **2009**, *29*, 2969–2978. [CrossRef]
155. Leilei, Z.; Hejun, L.; Shoujie, L.; Shaoxian, L.; Lina, P.; Yao, G.; Yulei, Z. In situ grown Si_3N_4 microbelt/Mg doped hydroxyapatite dual-layer coating on carbon/carbon composites for biomedical application. *Mater. Lett.* **2017**, *194*, 70–73. [CrossRef]
156. Vranceanu, D.M.; Ionescu, I.C.; Ungureanu, E.; Cojocaru, M.O.; Vladescu, A.; Cotrut, C.M. Magnesium doped hydroxyapatite-based coatings obtained by pulsed galvanostatic electrochemical deposition with adjustable electrochemical behavior. *Coatings* **2020**, *10*, 727. [CrossRef]
157. Huang, Y.; Qiao, H.; Nian, X.; Zhang, X.; Zhang, X.; Song, G.; Xu, Z.; Zhang, H.; Han, S. Improving the bioactivity and corrosion resistance properties of electrodeposited hydroxyapatite coating by dual doping of bivalent strontium and manganese ion. *Surf. Coat. Technol.* **2016**, *291*, 205–215. [CrossRef]
158. Huang, Y.; Ding, Q.; Han, S.; Yan, Y.; Pang, X. Characterisation, corrosion resistance and in vitro bioactivity of manganese-doped hydroxyapatite films electrodeposited on titanium. *J. Mater. Sci.–Mater. Med.* **2013**, *24*, 1853–1864. [CrossRef]
159. Pilmane, M.; Salma-Ancane, K.; Loca, D.; Locs, J.; Berzina-Cimdina, L. Strontium and strontium ranelate: Historical review of some of their functions. *Mater. Sci. Eng. C* **2017**, *78*, 1222–1230. [CrossRef]
160. Boanini, E.; Torricelli, P.; Fini, M.; Bigi, A. Osteopenic bone cell response to strontium-substituted hydroxyapatite. *J. Mater. Sci.–Mater. Med.* **2011**, *22*, 2079–2088. [CrossRef]
161. Schmidt, R.; Gebert, A.; Schumacher, M.; Hoffmann, V.; Voss, A.; Pilz, S.; Uhlemann, M.; Lode, A.; Gelinsky, M. Electrodeposition of Sr-substituted hydroxyapatite on low modulus beta-type Ti-45Nb and effect on in vitro Sr release and cell response. *Mater. Sci. Eng. C* **2020**, *108*, 110425. [CrossRef]
162. Drevet, R.; Benhayoune, H.; Michel, J. Structural characterization of electrodeposited strontium substituted calcium phosphate coatings. *J. Biomater. Tissue Eng.* **2011**, *1*, 68–75. [CrossRef]

163. Drevet, R.; Benhayoune, H. Pulsed electrodeposition for the synthesis of strontium-substituted calcium phosphate coatings with improved dissolution properties. *Mater. Sci. Eng. C* **2013**, *33*, 4260–4265. [CrossRef]
164. Tang, Y.; Chappell, H.F.; Dove, M.T.; Reeder, R.J.; Lee, Y.J. Zinc incorporation into hydroxylapatite. *Biomaterials* **2009**, *30*, 2864–2872. [CrossRef]
165. Huang, Y.; Zhang, X.; Mao, H.; Li, T.; Zhao, R.; Yan, Y.; Pang, X. Osteoblastic cell responses and antibacterial efficacy of Cu/Zn co-substituted hydroxyapatite coatings on pure titanium using electrodeposition method. *RSC Adv.* **2015**, *5*, 17076–17086. [CrossRef]
166. Furko, M.; Jiang, Y.; Wilkins, T.; Balázsi, C. Development and characterization of silver and zinc doped bioceramic layer on metallic implant materials for orthopedic application. *Ceram. Int.* **2016**, *42*, 4924–4931. [CrossRef]
167. Suelter, C.H. Enzymes Activated by Monovalent Cations. *Science* **1970**, *168*, 790. [CrossRef] [PubMed]
168. Wiesmann, H.P.; Plate, U.; Zierold, K.; Höhling, H.J. Potassium is Involved in Apatite Biomineralization. *J. Dent. Res.* **1998**, *77*, 1654–1657. [CrossRef]
169. Kumar, M.; Dasarathy, H.; Riley, C. Electrodeposition of brushite coatings and their transformation to hydroxyapatite in aqueous solutions. *J. Biomed. Mater. Res.* **1999**, *45*, 302–310. [CrossRef]
170. Matsunaga, K.; Murata, H. Formation Energies of Substitutional Sodium and Potassium in Hydroxyapatite. *Mater. Trans.* **2009**, *50*, 1041–1045. [CrossRef]
171. Kannan, S.; Ventura, J.M.G.; Ferreira, J.M.F. Synthesis and thermal stability of potassium substituted hydroxyapatites and hydroxyapatite/β-tricalcium phosphate mixtures. *Ceram. Int.* **2007**, *33*, 1489–1494. [CrossRef]
172. Kumar, M.; Xie, J.; Chittur, K.; Riley, C. Transformation of modified brushite to hydroxyapatite in aqueous solution: Effects of potassium substitution. *Biomaterials* **1999**, *20*, 1389–1399. [CrossRef]
173. Chen, K.; Ustriyana, P.; Moore, F.; Sahai, N. Biological Response of and Blood Plasma Protein Adsorption on Silver-Doped Hydroxyapatite. *ACS Biomater. Sci. Eng.* **2019**, *5*, 561–571. [CrossRef]
174. Shirkhanzadeh, M.; Azadegan, M.; Liu, G.Q. Bioactive delivery systems for the slow release of antibiotics: Incorporation of Ag^+ ions into micro-porous hydroxyapatite coatings. *Mater. Lett.* **1995**, *24*, 7–12. [CrossRef]
175. Mokabber, T.; Cao, H.T.; Norouzi, N.; van Rijn, P.; Pei, Y.T. Antimicrobial Electrodeposited Silver-Containing Calcium Phosphate Coatings. *ACS Appl. Mater. Interfaces* **2020**, *12*, 5531–5541. [CrossRef] [PubMed]
176. Li, H.; Zhao, X.; Cao, S.; Li, K.; Chen, M.; Xu, Z.; Lu, J.; Zhang, L. Na-doped hydroxyapatite coating on carbon/carbon composites: Preparation, in vitro bioactivity and biocompatibility. *Appl. Surf. Sci.* **2012**, *263*, 163–173. [CrossRef]
177. Vo, T.H.; Le, T.D.; Pham, T.N.; Nguyen, T.T.; Nguyen, T.P.; Dinh, T.M.T. Electrodeposition and characterization of hydroxyapatite coatings doped by Sr^{2+}, Mg^{2+}, Na^+ and F^- on 316L stainless steel. *Adv. Nat. Sci. Nanosci. Nanotechnol.* **2018**, *9*, 045001. [CrossRef]
178. Liu, S.; Li, H.; Zhang, L.; Yin, X.; Guo, Y. In simulated body fluid performance of polymorphic apatite coatings synthesized by pulsed electrodeposition. *Mater. Sci. Eng. C* **2017**, *79*, 100–107. [CrossRef]
179. Zhang, L.; Li, H.; Li, K.; Song, Q.; Fu, Q.; Zhang, Y.; Liu, S. Electrodeposition of carbonate-containing hydroxyapatite on carbon nanotubes/carbon fibers hybrid materials for tissue engineering application. *Ceram. Int.* **2015**, *41*, 4930–4935. [CrossRef]
180. Ge, X.; Zhao, J.; Lu, X.; Li, Z.; Wang, K.; Ren, F.; Wang, M.; Wang, Q.; Qian, B. Controllable phase transformation of fluoridated calcium phosphate ultrathin coatings for biomedical applications. *J. Alloys Compd.* **2020**, *847*, 155920. [CrossRef]
181. Wang, J.; Chao, Y.; Wan, Q.; Zhu, Z.; Yu, H. Fluoridated hydroxyapatite coatings on titanium obtained by electrochemical deposition. *Acta Biomater.* **2009**, *5*, 1798–1807. [CrossRef]
182. Aboudzadeh, N.; Dehghanian, C.; Shokrgozar, M.A. Effect of electrodeposition parameters and substrate on morphology of Si-HA coating. *Surf. Coat. Technol.* **2019**, *375*, 341–351. [CrossRef]
183. Dehghanian, C.; Aboudzadeh, N.; Shokrgozar, M.A. Characterization of silicon- substituted nano hydroxyapatite coating on magnesium alloy for biomaterial application. *Mater. Chem. Phys.* **2018**, *203*, 27–33. [CrossRef]
184. Graziani, G.; Boi, M.; Bianchi, M. A Review on Ionic Substitutions in Hydroxyapatite Thin Films: Towards Complete Biomimetism. *Coatings* **2018**, *8*, 269. [CrossRef]
185. Zhang, L.; Pei, L.; Li, H.; Li, S.; Liu, S.; Guo, Y. Preparation and characterization of Na and F co-doped hydroxyapatite coating reinforced by carbon nanotubes and SiC nanoparticles. *Mater. Lett.* **2018**, *218*, 161–164. [CrossRef]
186. Zhang, L.; Li, H.; Li, K.; Fu, Q.; Zhang, Y.; Liu, S. A Na and Si co-substituted carbonated hydroxyapatite coating for carbon nanotubes coated carbon/carbon composites. *Ceram. Int.* **2014**, *40*, 13123–13130. [CrossRef]
187. Liu, L.; Xiong, X.b.; Ma, J.; Ni, X.y.; Zeng, X.r.; Zeb Gul Sial, M.A.; Chen, D. Post-hydrothermal treatment of hydrothermal electrodeposited $CaHPO_4$ on C/C composites in sodium silicate-containing solution at various temperatures. *Ceram. Int.* **2019**, *45*, 5894–5903. [CrossRef]
188. Mumith, A.; Cheong, V.S.; Fromme, P.; Coathup, M.J.; Blunn, G.W. The effect of strontium and silicon substituted hydroxyapatite electrochemical coatings on bone ingrowth and osseointegration of selective laser sintered porous metal implants. *PLoS ONE* **2020**, *15*, e0227232. [CrossRef]
189. Robinson, L.; Salma-Ancane, K.; Stipniece, L.; Meenan, B.J.; Boyd, A.R. The deposition of strontium and zinc Co-substituted hydroxyapatite coatings. *J. Mater. Sci. – Mater. Med.* **2017**, *28*, 51. [CrossRef]
190. Wolf-Brandstetter, C.; Beutner, R.; Hess, R.; Bierbaum, S.; Wagner, K.; Scharnweber, D.; Gbureck, U.; Moseke, C. Multifunctional calcium phosphate based coatings on titanium implants with integrated trace elements. *Biomed. Mater.* **2020**, *15*, 025006. [CrossRef]

191. Liu, S.j.; Li, H.j.; Zhang, L.l.; Feng, L.; Yao, P. Strontium and magnesium substituted dicalcium phosphate dehydrate coating for carbon/carbon composites prepared by pulsed electrodeposition. *Appl. Surf. Sci.* **2015**, *359*, 288–292. [CrossRef]
192. Kolmas, J.; Groszyk, E.; Kwiatkowska-Rózycka, D. Substituted hydroxyapatites with antibacterial properties. *BioMed Res. Int.* **2014**, *2014*, 178123. [CrossRef]
193. Garbo, C.; Locs, J.; D'este, M.; Demazeau, G.; Mocanu, A.; Roman, C.; Horovitz, O.; Tomoaia-Cotisel, M. Advanced Mg, Zn, Sr, Si multi-substituted hydroxyapatites for bone regeneration. *Int. J. Nanomed.* **2020**, *15*, 1037–1058. [CrossRef]
194. Bracci, B.; Torricelli, P.; Panzavolta, S.; Boanini, E.; Giardino, R.; Bigi, A. Effect of Mg^{2+}, Sr^{2+}, and Mn^{2+} on the chemico-physical and in vitro biological properties of calcium phosphate biomimetic coatings. *J. Inorg. Biochem.* **2009**, *103*, 1666–1674. [CrossRef]
195. Furko, M.; Jiang, Y.; Wilkins, T.A.; Balázsi, C. Electrochemical and morphological investigation of silver and zinc modified calcium phosphate bioceramic coatings on metallic implant materials. *Mater. Sci. Eng. C* **2016**, *62*, 249–259. [CrossRef] [PubMed]
196. Furko, M.; May, Z.; Havasi, V.; Kónya, Z.; Grünewald, A.; Detsch, R.; Boccaccini, A.R.; Balázsi, C. Pulse electrodeposition and characterization of non-continuous, multi-element-doped hydroxyapatite bioceramic coatings. *J. Solid State Electrochem.* **2018**, *22*, 555–566. [CrossRef]
197. Furko, M.; Della Bella, E.; Fini, M.; Balázsi, C. Corrosion and biocompatibility examination of multi-element modified calcium phosphate bioceramic layers. *Mater. Sci. Eng. C* **2019**, *95*, 381–388. [CrossRef]
198. Huang, Y.; Ding, Q.; Pang, X.; Han, S.; Yan, Y. Corrosion behavior and biocompatibility of strontium and fluorine co-doped electrodeposited hydroxyapatite coatings. *Appl. Surf. Sci.* **2013**, *282*, 456–462. [CrossRef]
199. Bir, F.; Khireddine, H.; Mekhalif, Z.; Bonnamy, S. Pulsed electrodeposition of Ag^{+} doped prosthetic Fluorohydroxyapatite coatings on stainless steel substrates. *Mater. Sci. Eng. C* **2021**, *118*, 111325. [CrossRef] [PubMed]
200. Vahabzadeh, S.; Bose, S. Effects of Iron on Physical and Mechanical Properties, and Osteoblast Cell Interaction in β-Tricalcium Phosphate. *Ann. Biomed. Eng.* **2017**, *45*, 819–828. [CrossRef] [PubMed]
201. Singh, R.K.; Srivastava, M.; Prasad, N.K.; Awasthi, S.; Dhayalan, A.; Kannan, S. Iron doped β-Tricalcium phosphate: Synthesis, characterization, hyperthermia effect, biocompatibility and mechanical evaluation. *Mater. Sci. Eng. C* **2017**, *78*, 715–726. [CrossRef]
202. Singh, R.K.; Srivastava, M.; Prasad, N.K.; Shetty, P.H.; Kannan, S. Hyperthermia effect and antibacterial efficacy of Fe^{3+}/Co^{2+} co-substitutions in β-$Ca_3(PO_4)_2$ for bone cancer and defect therapy. *J. Biomed. Mater. Res. B* **2018**, *106*, 1317–1328. [CrossRef]
203. Demnati, I.; Grossin, D.; Combes, C.; Parco, M.; Braceras, I.; Rey, C. A comparative physico-chemical study of chlorapatite and hydroxyapatite: From powders to plasma sprayed thin coatings. *Biomed. Mater.* **2012**, *7*, 054101. [CrossRef]
204. Navarrete-Segado, P.; Frances, C.; Tourbin, M.; Tenailleau, C.; Duployer, B.; Grossin, D. Powder bed selective laser process (sintering/melting) applied to tailored calcium phosphate-based powders. *Addit. Manuf.* **2022**, *50*, 102542. [CrossRef]
205. Chen, X.; Hill, R.; Karpukhina, N. Chlorapatite Glass-Ceramics. *Int. J. Appl. Glass Sci.* **2014**, *5*, 207–216. [CrossRef]
206. Pan, C.; Chen, L.; Wu, R.; Shan, H.; Zhou, Z.; Lin, Y.; Yu, X.; Yan, L.; Wu, C. Lithium-containing biomaterials inhibit osteoclastogenesis of macrophages in vitro and osteolysis in vivo. *J. Mater. Chem. B* **2018**, *6*, 8115–8126. [CrossRef] [PubMed]
207. Wang, Y.; Yang, X.; Gu, Z.; Qin, H.; Li, L.; Liu, J.; Yu, X. In vitro study on the degradation of lithium-doped hydroxyapatite for bone tissue engineering scaffold. *Mater. Sci. Eng. C* **2016**, *66*, 185–192. [CrossRef]
208. Lin, Y.; Yang, Z.; Cheng, J. Preparation, Characterization and Antibacterial Property of Cerium Substituted Hydroxyapatite Nanoparticles. *J. Rare Earths* **2007**, *25*, 452–456. [CrossRef]
209. Feng, Z.; Liao, Y.; Ye, M. Synthesis and structure of cerium-substituted hydroxyapatite. *J. Mater. Sci.–Mater. Med.* **2005**, *16*, 417–421. [CrossRef]
210. El Khouri, A.; Zegzouti, A.; Elaatmani, M.; Capitelli, F. Bismuth-substituted hydroxyapatite ceramics synthesis: Morphological, structural, vibrational and dielectric properties. *Inorg. Chem. Commun.* **2019**, *110*, 107568. [CrossRef]
211. Ciobanu, G.; Bargan, A.M.; Luca, C. New Bismuth-Substituted Hydroxyapatite Nanoparticles for Bone Tissue Engineering. *JOM* **2015**, *67*, 2534–2542. [CrossRef]
212. Melnikov, P.; Teixeira, A.R.; Malzac, A.; Coelho, M.d.B. Gallium-containing hydroxyapatite for potential use in orthopedics. *Mater. Chem. Phys.* **2009**, *117*, 86–90. [CrossRef]
213. Korbas, M.; Rokita, E.; Meyer-Klaucke, W.; Ryczek, J. Bone tissue incorporates in vitro gallium with a local structure similar to gallium-doped brushite. *J. Biol. Inorg. Chem.* **2004**, *9*, 67–76. [CrossRef]
214. Wang, Y.; Wang, J.; Hao, H.; Cai, M.; Wang, S.; Ma, J.; Li, Y.; Mao, C.; Zhang, S. In Vitro and in Vivo Mechanism of Bone Tumor Inhibition by Selenium-Doped Bone Mineral Nanoparticles. *ACS Nano* **2016**, *10*, 9927–9937. [CrossRef]
215. Rodríguez-Valencia, C.; López-Álvarez, M.; Cochón-Cores, B.; Pereiro, I.; Serra, J.; González, P. Novel selenium-doped hydroxyapatite coatings for biomedical applications. *J. Biomed. Mater. Res. A* **2013**, *101*, 853–861. [CrossRef] [PubMed]
216. Tan, H.W.; Mo, H.Y.; Lau, A.T.Y.; Xu, Y.M. Selenium species: Current status and potentials in cancer prevention and therapy. *Int. J. Mol. Sci.* **2019**, *20*, 75. [CrossRef] [PubMed]
217. Alshemary, A.Z.; Akram, M.; Goh, Y.F.; Abdul Kadir, M.R.; Abdolahi, A.; Hussain, R. Structural characterization, optical properties and in vitro bioactivity of mesoporous erbium-doped hydroxyapatite. *J. Alloys Compd.* **2015**, *645*, 478–486. [CrossRef]
218. Neacsu, I.A.; Stoica, A.E.; Vasile, B.S.; Andronescu, E. Luminescent hydroxyapatite doped with rare earth elements for biomedical applications. *Nanomaterials* **2019**, *9*, 239. [CrossRef] [PubMed]
219. Pham, V.H.; Van, H.N.; Tam, P.D.; Ha, H.N.T. A novel 1540 nm light emission from erbium doped hydroxyapatite/β-tricalcium phosphate through co-precipitation method. *Mater. Lett.* **2016**, *167*, 145–147. [CrossRef]

220. Yang, P.; Quan, Z.; Li, C.; Kang, X.; Lian, H.; Lin, J. Bioactive, luminescent and mesoporous europium-doped hydroxyapatite as a drug carrier. *Biomaterials* **2008**, *29*, 4341–4347. [CrossRef]
221. Al-Kattan, A.; Santran, V.; Dufour, P.; Dexpert-Ghys, J.; Drouet, C. Novel contributions on luminescent apatite-based colloids intended for medical imaging. *J. Biomater. Appl.* **2014**, *28*, 697–707. [CrossRef]
222. Paduraru, A.V.; Oprea, O.; Musuc, A.M.; Vasile, B.S.; Iordache, F.; Andronescu, E. Influence of Terbium Ions and Their Concentration on the Photoluminescence Properties of Hydroxyapatite for Biomedical Applications. *Nanomaterials* **2021**, *11*, 2442. [CrossRef]